PERGAMON

Journal of Structural Geology 25 (2003) 1049–1081

JOURNAL OF STRUCTURAL GEOLOGY

www.elsevier.com/locate/jsg

Structure of the Kaoko Belt, Namibia: progressive evolution of a classic transpressional orogen

Ben Goscombe[a,*], Martin Hand[a], David Gray[b,1]

[a]*Department of Geology and Geophysics, Adelaide University, Adelaide, South Australia, 5005, Australia*
[b]*School of Geosciences, Monash University, Melbourne, Victoria, 3800, Australia*

Received 10 December 2001; received in revised form 10 May 2002; accepted 16 August 2002

Abstract

The Kaoko Belt portion of the Damara Orogen, Namibia, is the deeply eroded core of a sinistral transpressional orogen that has half-flower structure geometry centred on the major, 4–5-km-wide Purros Mylonite Zone. Formed between the Congo Craton in the east and Rio De La Plata Craton in Brazil, the Kaoko Belt represents the northern coastal arm of a triple junction within the Pan-African Orogenic System. Consisting of reworked Archaean, Palaeoproterozoic and Mesoproterozoic basement and a cover of Neoproterozoic Damara Sequence, the Kaoko Belt can be sub-divided structurally into three parallel NNW-trending zones. The Eastern Kaoko Zone comprises sub-greenschist facies shelf carbonates that have been uprightly folded. The Central Kaoko Zone contains a slope and deep basin facies succession that has experienced intense deformation, including pervasive reworking of basement into large-scale east-vergent nappes. The Western Kaoko Zone is predominantly deep basin facies of high metamorphic grade intruded by numerous granites. It has experienced intense wrench-style deformation with formation of upright isoclines and steep, crustal-scale shear zones. The Kaoko Belt evolved through three distinct phases of a protracted Pan-African Orogeny in the late Neoproterozoic to Cambrian. (1) An early *Thermal Phase* (M_1) was responsible for pervasive partial melting and granite emplacement in the Western Kaoko Zone from 656 Ma. (2) The *Transpressional Phase* produced the geometry of the belt by progressive sinistral shearing between 580 and 550 Ma. Deformation was continuously progressive through two stages and involved both temporal and spatial migration of deformation outwards towards the margin. The early strike-slip Wrench-Stage produced a high-strain L–S fabric by sub-horizontal transport. Deformation became progressively more transpressive, with high-angle convergence and flattening strains during the Convergent-Stage. In this stage, strike-slip movements evolved through multiple fold generations, progressively steeper stretching lineations, west over east verging large-scale nappes and overfolds and ultimately thrusts with shortening at a high-angle to the orogen. The pervasive L-S fabric was continually reworked and was both folded by nappes and partitioned into sub-vertical crustal-scale shear zones forming at the same time in the core of the orogen. (3) A post-transpression *Shortening Phase*, with large-scale, upright, open folds formed during minor N–S shortening along the length of the belt (a phase of deformation correlated with high-angle convergence in the Inland Branch of the Damara Orogen at 530–510 Ma).

Keywords: Namibia; Pan-African Orogeny; Orogen architecture; Transpression; Shear zone; Damara Orogen

1. Introduction

Orogens involving oblique convergence are now believed to be an important part of collisional orogenic systems (Jones et al., 1977; Woodcock, 1986; Holdsworth and Strachan, 1991; Jones and Strachan, 2000). Most studies of oblique convergence orogens with strike-slip and transpressional components are from the brittle upper-crust (Harland, 1971; Lowell, 1972; Wilcox et al., 1973; Sylvester and Smith, 1976; Sylvester, 1988; Oldow et al., 1990; Holdsworth and Pinheiro, 2000). Studies of transpressional systems in the middle-crust come from orogen-scale examples (Hansen, 1989; Holdsworth and Strachan, 1991; Little et al., 2002) and discrete shear zones (Tikoff and Greene, 1997; Johnson and Kattan, 2001; Lin and Jiang, 2001). There are few studies from deeply eroded transpressional orogens representing the ductile lower crust (Vassallo and Wilson, 2002). The data

* Corresponding author. Present address: School of Earth and Environmental Sciences, College of Natural Sciences, Seoul National University, Seoul 151-742, Korea.
E-mail addresses: bgoscombe@snu.ac.kr (B. Goscombe), m.hand@adelaide.edu.au (M. Hand), dgray@earth.monash.edu.au (D. Gray).
[1] Now at: School of Earth Sciences, University of Melbourne, Melbourne, Victoria, 3010, Australia.

0191-8141/03/$ - see front matter © 2002 Elsevier Science Ltd. All rights reserved.
PII: S0191-8141(02)00150-5

available worldwide from middle- and lower-crust exposures of transpressional orogens suggests a common strain distribution across such belts, incorporating strike-slip shearing in the internal part of the orogen, often with a major crustal-scale median shear zone, through progressively more oblique convergence to high-angle over-thrusting onto the foreland. Classic orogen-scale examples include the Caledonian Orogen in NE Greenland (Holdsworth and Strachan, 1991), the Pan-African Mozambique Belt (Shackleton and Ries, 1984) and Pan-African Kaoko Belt in Namibia—the subject of this study.

The Kaoko Belt is characterized by all the typical features of an oblique convergent orogen in the middle- to lower-crust. These include: colinear folds and stretching lineations, high plane to flattening strains, progressive deformation to higher angle overthrusting at the margins and a median crustal-scale strike-slip shear zone in the core of the orogen. Furthermore, the entire orogen is well exposed and contains different styles of basement reactivation and cover deformation from sub-greenschist grade in the foreland to granulite grade in the hinterland. Until very recently the Kaoko Belt was poorly understood and largely unmapped (Guj, 1970), because of its remoteness and the security problems in northern Namibia throughout the 1970s and '80s. Recently, geological studies have presented preliminary frameworks for structural evolution (Guj, 1970; Dingeldey et al., 1994; Dürr and Dingeldey, 1996; Dingeldey, 1997), metamorphism (Dingeldey, 1997) and geochronology (Ahrendt et al., 1983; Seth et al., 1998).

We present the first structural analysis of the entire Kaoko Belt, document previously unrecognised crustal-scale structures and establish the architecture of this classic example of a transpressional orogen. This study reconstructs the deformation history and tectonic framework (Table 1) as part of a larger tectono-metamorphic study. The geochronology of matrix assemblages and metamorphic evolution are presented in Goscombe et al. (2002). Our analysis is based on six field seasons (1997–2002), involving reconnaissance observations throughout the entire Kaoko Belt and north Namibia region, detailed Orumpembe, Hoanib and Ugab traverses (Fig. 1) and detailed mapping of a 30-km-wide swath across the belt (Fig. 1; Goscombe, 1999b,c,d,e). Our mapping is supplemented in the southern Kaoko Belt region (Hoanib traverse) by the work of Guj (1970), Dingeldey et al. (1994), Dürr and Dingeldey (1996), Dingeldey (1997) and Seth et al. (1998). Structural analysis of the entire Kaoko Belt was undertaken using comprehensive data sets that we have compiled from geological mapping, structural data (16,500 structural readings), age dating (Appendix A) and petrological data (1600 samples). These data were sourced from our work and both published and unpublished maps and reports and form the basis of simplified structural, chronostratigraphic and metamorphic maps covering the entire Kaoko Belt.

2. Regional geology of the Kaoko Belt

The Neoproterozoic Damara Orogen within Namibia has triple junction geometry (Fig. 1). The Kaoko Belt is the NNW-trending northern coastal arm that extends 700 km from the Ugab Zone in the south to Angola in the North (Fig. 1). The Gariep Belt is the N-trending southern coastal arm (Davies and Coward, 1982; Frimmel, 1995; Hälbich and Alchin, 1995) and the Inland Branch trends ENE–WSW into Botswana (Coward, 1981; Miller, 1983; Porada et al., 1983) (Fig. 1). The relationship between the Kaoko Belt and the continent-scale network of late Neoproterozoic to early Palaeozoic orogenic belts called the Pan-African Orogenic System (PAOS) (Goscombe et al., 2000) is summarized in Fig. 1. In the Kaoko Belt, the Neoproterozoic Damara Sequence unconformably overlies a mosaic of Archaean, Palaeoproterozoic and Mesoproterozoic basement metamorphic and igneous complexes that form the southwest margin of the otherwise predominantly Archaean Congo Craton. The western margin equivalent of the Kaoko Belt in Brazil consists of the sinistral transpressional Dom Feliciano and Ribeira Belts flanking the Rio De La Plata Craton (Porada, 1989; Chemale et al., 1994; Trompette and Carozzi, 1994). Deposition of the Damara Sequence was terminated by collision late in the Neoproterozoic and was followed by a protracted period of tectonothermal events collectively called the Damara Orogeny, from the late Neoproterozoic to Cambrian (Miller, 1983; Prave, 1996) (Table 1).

The Kaoko Belt can be sub-divided into three elongate NNW-trending, shear zone-bounded zones with distinct stratigraphy and characteristic tectonic and metamorphic style (Miller, 1983) (Figs. 1 and 2):

1. The Eastern Kaoko Zone (EKZ) is the foreland, comprising sub-greenschist facies Damara Sequence platform carbonates resting on the western margin of the Congo Craton, the Palaeoproterozoic Kamanjab Inlier in the south and Epupa Metamorphic Complex in the north. Deformation involved early schistose foliation development overprinted by the dominant late-stage E–W shortening and upright folds. The western margin of the EKZ is marked by the shallowly west-dipping Sesfontein Thrust (Figs. 2 and 3), which formed under brittle conditions late in the Damara orogenic cycle.
2. The Central Kaoko Zone (CKZ) consists of Damara Sequence of deep basin and slope facies, ranging in grade from lower-greenschist facies in the east to upper-amphibolite facies in the west. The CKZ experienced intense fabric development in both basement and cover during sinistral transpression, culminating in large-scale east-vergent nappes. The western margin is delineated by the Purros Mylonite Zone (PMZ) (Goscombe, 1998; Goscombe and Hand, 2001), a crustal-scale, upper-amphibolite mylonite and ultra-mylonite zone (Fig. 3). The PMZ is a sub-vertical median shear zone running the

Table 1
Tectono-metamorphic events recognized in the Kaoko Belt

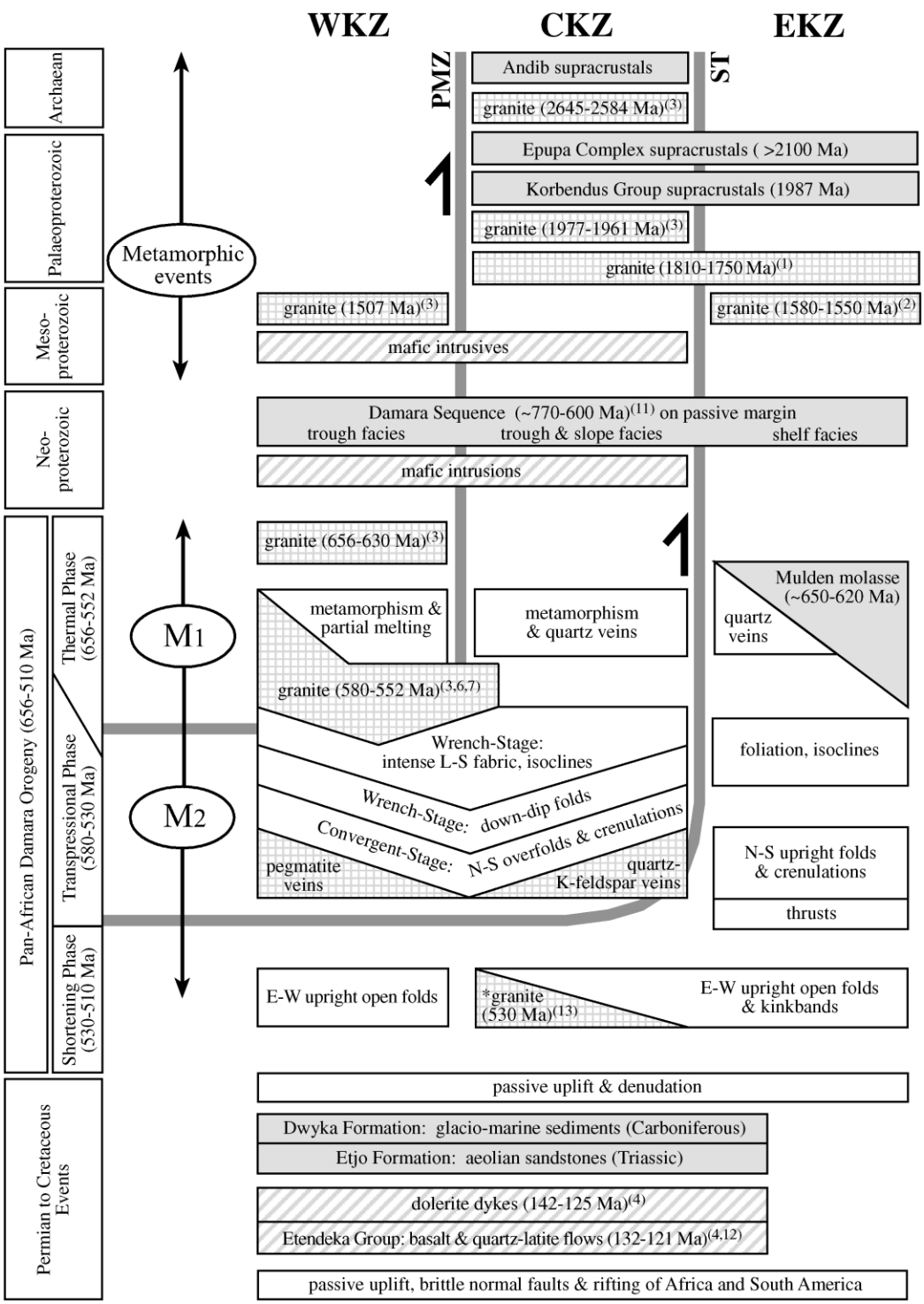

Age ranges from literature as discussed in text and numbered as in Appendix A. Chrono-spatial position of Purros Mylonite Zone (PMZ) and Sesfontain Thrust (ST) indicated by shaded lines. *Only in southern Kaoko Belt (Ugab Zone).

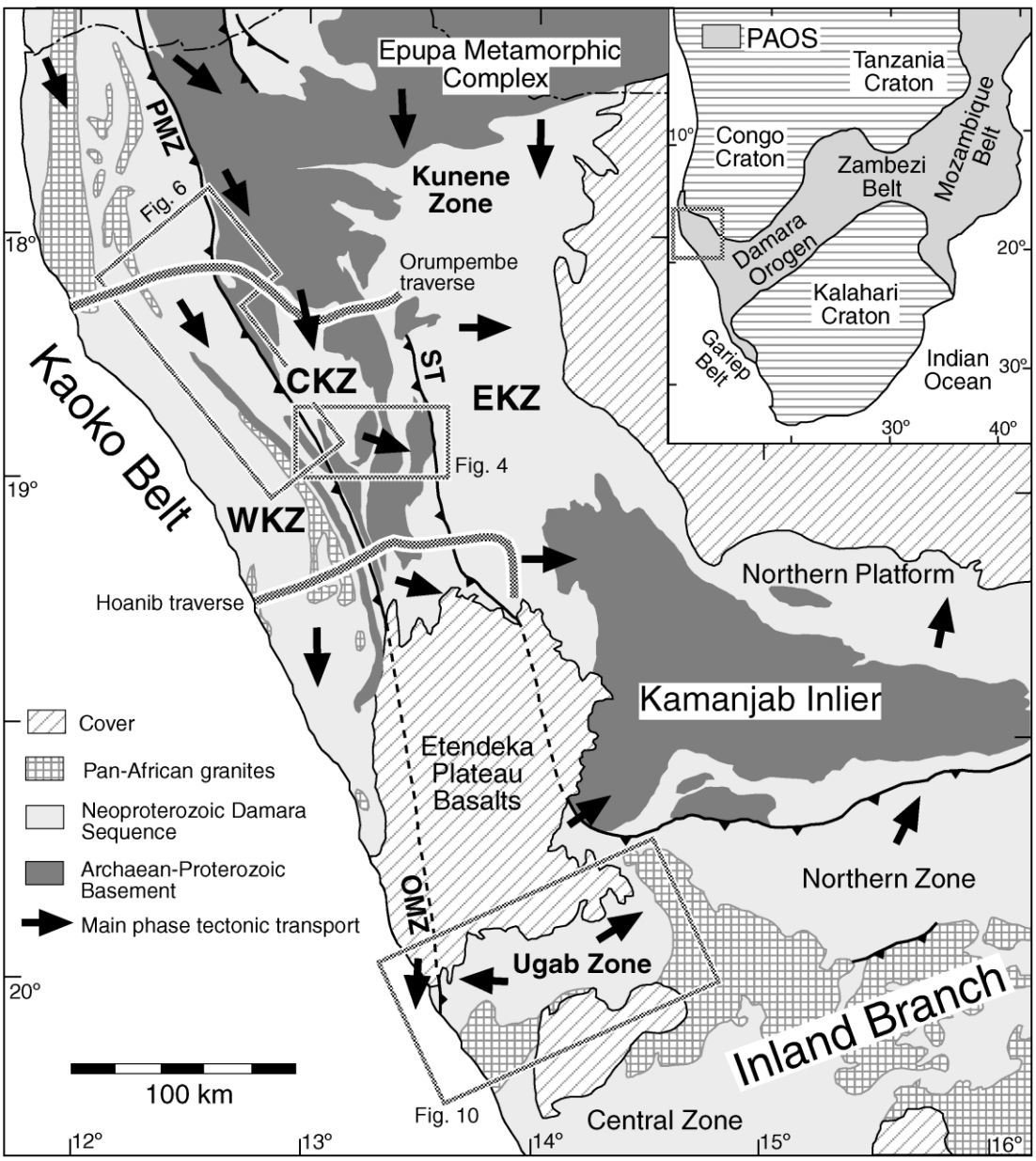

Fig. 1. Location map of the Kaoko Belt branch of the Damara Orogen. The inset outlines the regional context within the Cambrian Pan-African Orogenic System (PAOS), after Goscombe et al. (2000). Boxes outline areas mapped in detail, and solid lines indicate traverses investigated. ST—Sesfontain Thrust; PMZ—Purros Mylonite Zone; OMZ—Ogden Mylonite Zone; EKZ—Eastern Kaoko Zone; CKZ—Central Kaoko Zone; WKZ—Western Kaoko Zone. Arrows indicate upper-plate transport direction during the main phase of the Damara Orogeny in different regions. These are not necessarily time equivalent and are based on stretching lineations in highly sheared regions and fold vergence in regions devoid of stretching lineations (i.e. Ugab Zone, EKZ and Kunene Zone).

entire length of the Kaoko Belt, north into Angola and south of the Etendeka Plateau is exposed as the Ogden mylonites (Miller, 1983) on the west margin of the Ugab Zone (Fig. 1).

3. The Western Kaoko Zone (WKZ) is dominated by amphibolite- to granulite-grade Damara Sequence with a high proportion of partial melt and Pan-African granites, and few pre-Damara basement antiformal slivers exposed only in the eastern part of the WKZ (Figs. 1 and 3). Structural style is characterized by steep, sinistral crustal-scale shear zones and panels of isoclinally folded rocks that range from very steep easterly inclination adjacent to the PMZ, through vertical to shallowly west-inclined at the coast.

The Kaoko Belt is terminated to the northeast and south by distinct zones that similarly can be structurally characterized:

1. The Kunene Zone at the northeast margin of the Kaoko Belt (Fig. 1) is dominated by Palaeoproterozoic and Mesoproterozoic basement with low-grade platform Damara Sequence. Deformation involved N–S shortening without transpression, and was expressed as steep

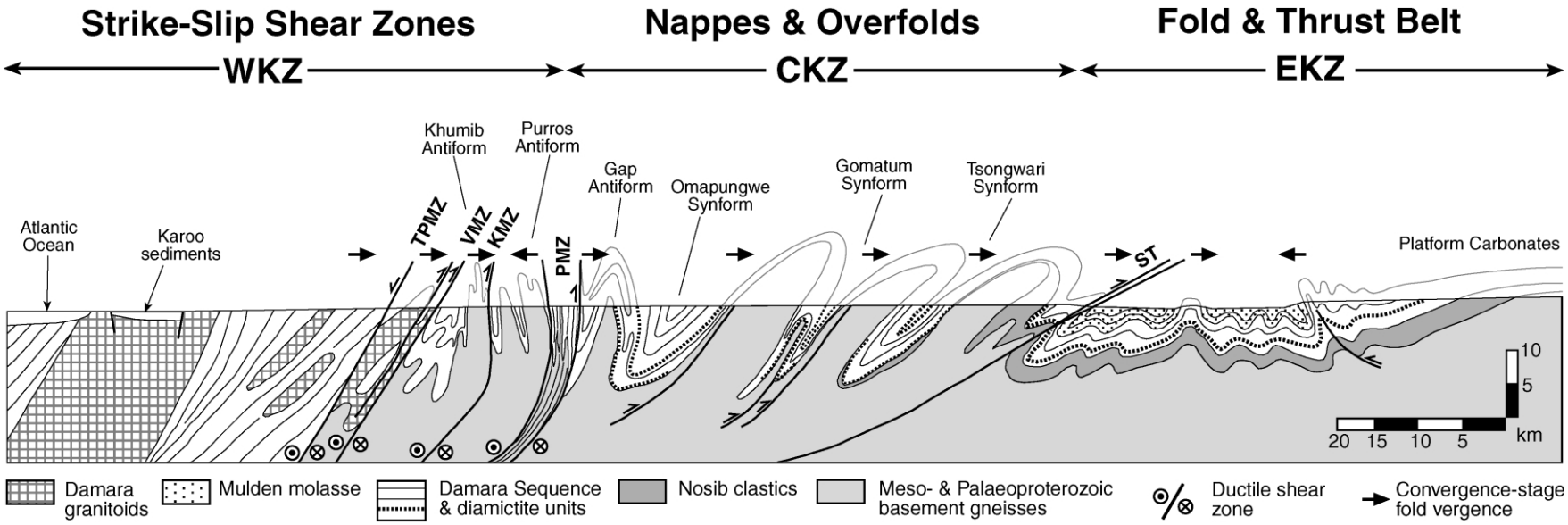

Fig. 2. Schematic cross-section across the entire Kaoko Belt (Fig. 3), centred on the areas mapped in detail (Figs. 4 and 6). Abbreviations as in Fig. 1 and KMZ—Khumib Mylonite Zone; VMZ—Village Mylonite Zone; TPMZ—Three Palms Mylonite Zone.

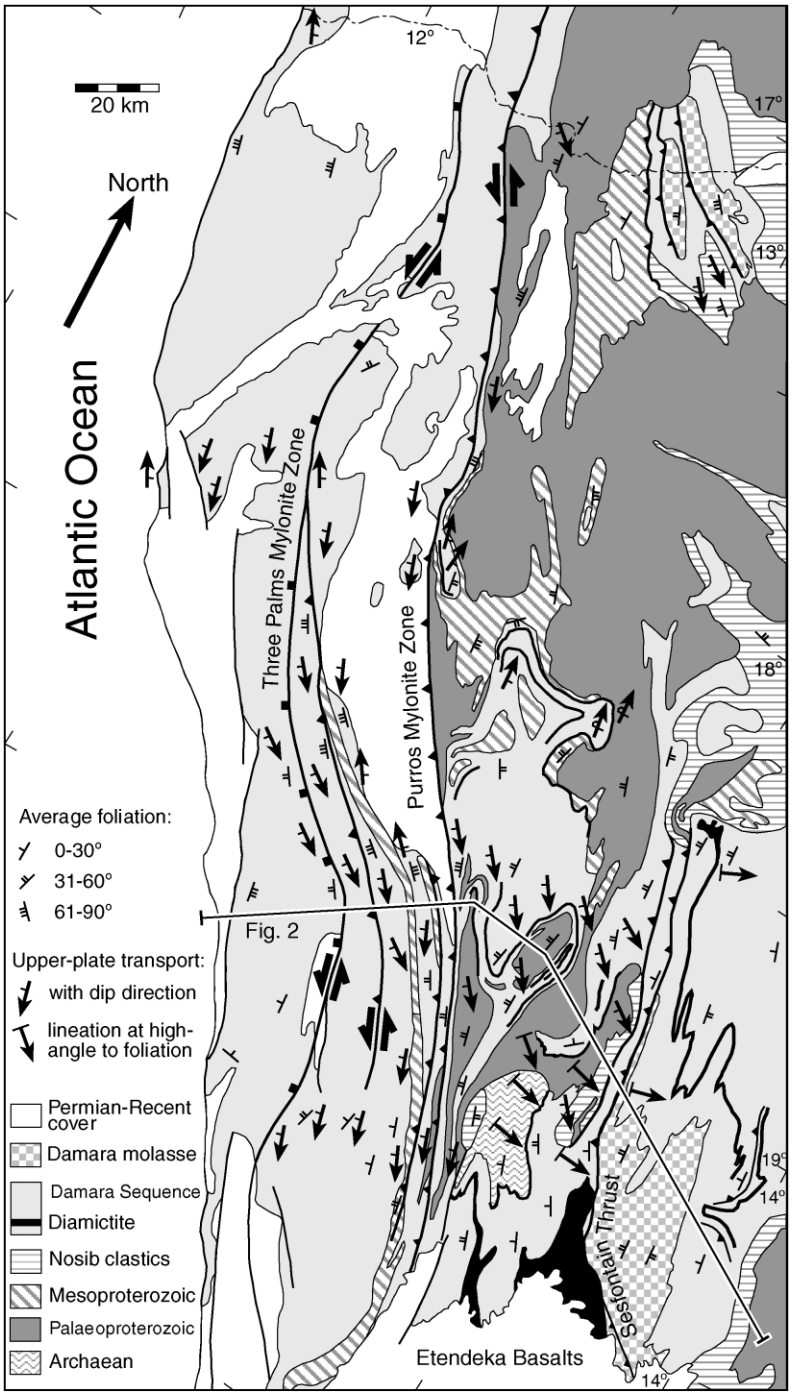

Fig. 3. Tectonic map of the Kaoko Belt indicating the major chronostratigraphic rock units, the median PMZ and tectonic transport directions during the Transpressional Phase of the Damara Orogeny. Average orientation of the pervasive foliation from domains covering the entire Kaoko Belt are indicated and based on a data set of 16,500 readings from published and unpublished maps and papers and the authors data. Trace of cross-section (Fig. 2) indicated.

retrograde shear zones in basement and upright E- to ESE-trending folds in the Damara Sequence.

2. The southern-most extension of the Kaoko Belt is the Ugab Zone (Fig. 1). The Ugab Zone is comprised of a thin turbiditic Damara Sequence of greenschist facies grade that has been pervasively deformed by very tight chevron folding without involvement of the basement (Freyer and Halbich, 1994).

3. Chronostratigraphic rock units

3.1. Archaean to Mesoproterozoic—pre-Damara basement

The Damara Sequence is underlain by a mosaic of basement terranes of different age and character (Table 1), all representing the southwest margin of the Congo Craton (Fig. 1). Archaean orthogneisses of approximately 2645–

2585 Ma age (Seth et al., 1998), are restricted to a single CKZ antiformal nappe, outcropping in the Hoanib traverse (Figs. 1 and 2). Palaeoproterozoic age basement dominates the CKZ, EKZ and platform regions. High-grade Palaeoproterozoic gneisses in the north and central Kaoko Belt region have been named the Epupa Metamorphic Complex (Fig. 1), which is thought to be of >2100 Ma age (Miller, 1983) and contains granitic orthogneisses of approximately 1795 ± 30 Ma age (Tegtmeyer and Kroner, 1985). Palaeoproterozoic gneisses in CKZ antiformal nappes comprise a variable supracrustal suite of quartzo-feldspathic paragneisses, meta-quartzite, mafic gneiss and meta-pelite, with granitic orthogneisses (Fig. 4) of approximately 1985–1961 Ma age (Seth et al., 1998). The Kamanjab Inlier to the southeast (Fig. 1), is comprised of metamorphic sequences of 1987 ± 4 and 1811 ± 35 Ma age (Tegtmeyer and Kroner, 1985) and granites of approximately 1800 ± 80 and 1580–1547 Ma age (Burger et al., 1976) (Table 1). Two distinct Mesoproterozoic suites are recognised in the Kaoko Belt. A supracrustal sequence dominated by meta-quartzites and amphibolites, unconformably overlies the Epupa Metamorphic Complex (Miller, 1983) and is restricted to the northern CKZ and EKZ. Antiformal basement panels in the WKZ (Fig. 3) consist of a bimodal suite of meta-igneous mafic and felsic gneisses and paragneisses (Fig. 4). Zircons from the meta-igneous felsic gneisses give a SHRIMP age of 1507 ± 16 and evaporation age of 1335 ± 1 Ma (Seth et al., 1998). These basement lithologies and Mesoproterozoic ages are in contrast to those in the CKZ and indicate that the PMZ marks the boundary between two basement terranes of different age (Fig. 3).

3.2. Neoproterozoic cover—Damara Sequence

The Damara Sequence is a marine sequence of 770–600 Ma age (Miller, 1983; Hoffman, 1994; Frimmel, 1996; Prave, 1996), deposited on a passive margin, progressing from shelf carbonates in the EKZ (Hoffman et al., 1998) to slope and deep basin facies in the CKZ and WKZ. The basal Damara Sequence is represented by rift-related siliciclastics of the Nosib Group, which contains quartzites, conglomerates and arenites and upper limiting ages of approximately 750 Ma (Hoffman et al., 1994, 1996, 1998; Prave, 1996). The Nosib Group forms thick sequences throughout the EKZ and pinches out in the eastern CKZ (Fig. 2), indicating transition from shelf to slope facies at the margin between these zones. The Sesfontain Thrust (Fig. 1) marks the margin between the carbonate shelf and slope facies and a shear zone in the eastern Ugab Zone marks a similar transition (Swart, 1992). These shear zones may represent reactivated growth faults in the passive margin (Porada, 1979). The overlying Otavi Group is dominated by carbonates in the EKZ and in the CKZ and WKZ, by turbiditic meta-pelite, meta-greywacke and quartz-muscovite schist with subordinate mafic schists, calcsilicate, carbonate and quartzite (Figs. 4 and 6). Two diamictite units are recognised in the EKZ (Hoffman et al., 1998) and mapped across the CKZ as far as the PMZ (Figs. 3 and 4). These are correlated with those in the Inland Branch and Gariep Belt, of approximately 750–735 and 700 Ma age (Hoffman, 1994; Frimmel, 1996; Folling et al., 1998; Hoffman et al., 1998). Deposition terminated as the Mulden Group siliciclastic molasse of approximately 650–620 Ma age (Miller, 1983), which is only preserved east of the Sesfontain Thrust in the EKZ (Fig. 3; Guj, 1970).

3.3. Neoproterozoic and Palaeozoic (Pan-African) granites

Pan-African granites are common in the WKZ (contributing 20% of exposure), entirely absent from the EKZ and occur only as rare granitic veins (centimetre-scale) and granitic orthogneiss sills (metre-scale) in the western-most CKZ (Fig. 4). At least four generations of Pan-African granites and partial melting are recognised. The first two are strongly sheared and develop a pervasive L–S fabric, being emplaced either prior to, or during the main-phase of deformation in the Damara Orogeny (Table 1). (1) Dioritic orthogneiss with a zircon SHRIMP age of 656 ± 8 Ma (Seth et al., 1998) is only found in the western WKZ. (2) Large (kilometre-scale), lenticular granitic orthogneiss bodies dominate the WKZ (Fig. 6) and rarely preserve discordant intrusive contacts. The most common type is mega-crystic S-type granites with zircon evaporation ages ranging from 580 ± 3 to 552 ± 2 Ma (Seth et al., 1998) and granites from the southern Kaoko Belt have 570 ± 20 Ma zircon ages (Miller and Burger, 1983) and 573 ± 33 Ma Rb–Sr whole-rock ages (Kröner, 1982). These orthogneisses are associated with pervasive centimetre-scale stromatic partial melt segregations in the host rocks. (3) In high-grade portions of the WKZ, minor volumes of discordant pegmatite and micro-granite veins of centimetre-scale were emplaced axial planar to tight overturned folds formed in the Damara Orogeny (Table 1). (4) The southern extension of the Kaoko Belt (Ugab Zone) contains composite plutons that post-date pervasive deformation associated with transpression in the Kaoko Belt and were emplaced syn-kinematic with late-stage N–S shortening (Table 1). Pb–Pb single zircon evaporation ages, from two samples of the syenite core of the Voetspoor composite pluton, are 530 ± 3 Ma (Seth et al., 2000).

4. Tectonic framework

The temporal and spatial framework of deformational events recognised in the Kaoko Belt is summarized in Table 1. There is evidence, largely from the geochonological record (Burger et al., 1976; Tegtmeyer and Kroner, 1985; Seth et al., 1998), for multiple tectonothermal events in the various basement units prior to deposition of the Damara Sequence. Pre-Damara tectono-metamorphic cycles are further inferred by relic high-grade mineral

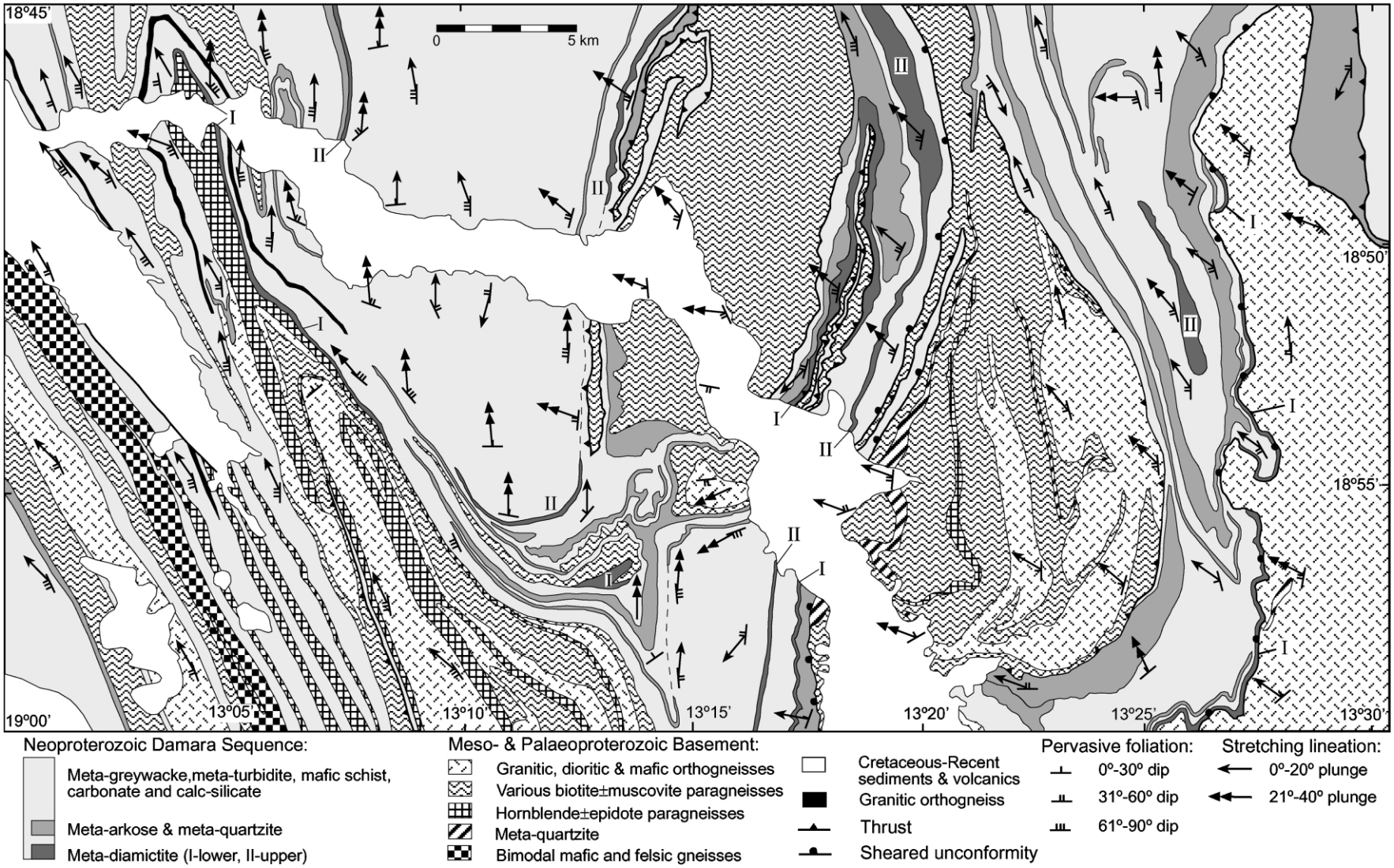

Fig. 4. Simplified geological map of the CKZ portion of the central profile. The numerous carbonate and amphibolite units in the Damara Sequence are not indicated for clarity. The central valley without rock exposure is a Permian glacial valley.

assemblages, strain-hardened textures, gneissic layering, partial melt segregations and Proterozoic granitoids. Proterozoic fabrics and high-grade mineral assemblages are preserved almost entirely un-reworked in basement exposures of the Northern Platform, EKZ and Kunene Zone (Fig. 1). Palaeoproterozoic gneisses have E–W-trending stretching lineations (Goscombe, 1999a) and the overlying Mesoproterozoic sequences have top-to-the-NNE transport along sub-horizontal stretching lineations. Within the WKZ and CKZ, basement antiforms were almost entirely ductilely recrystallized producing an intense L–S fabric during the Damara Orogeny. Consequently, little is known of pre-Damara kinematics and relic pre-Damara porphyroclasts from upper amphibolite grade assemblages are rarely preserved.

In common with other parts of the Pan-African Orogenic System (Goscombe et al., 2000), the Damara Orogeny is protracted, with tectonothermal events spanning approximately 660–510 Ma. Three distinct phases, as part of a progressive continuum, can be recognised within the Kaoko Belt specifically:

1. The *Thermal Phase* produced early metamorphism (M_1) of the Damara Sequence, with no apparent deformation structures preserved, and occurred prior to development of the pervasive L–S fabric and matrix mineral assemblages formed during the Transpressional Phase of the Damara Orogeny (M_2) (Table 1). Relic coarse-grained M_1 porphyroclasts of garnet, biotite, muscovite and hornblende are deformed, enveloped, boudinaged and grain-refined by the pervasive L–S fabric, indicating coarse mineral growth prior to the main deformational phase. The Thermal Phase is further evidenced by early hydrothermal quartz ± K-feldspar ± calcite ± muscovite veins in the CKZ and in the WKZ, by migmatization and granite emplacement with zircon evaporation minimum ages ranging from 656 ± 8 to 630 ± 8 Ma and 580 ± 3 to 552 ± 2 Ma (Seth et al., 1998; Appendix A). All veins, partial melt segregations and granites are boudinaged, show high degrees of grain-refinement and develop the regionally pervasive L–S fabric.
2. The architecture of the Kaoko Belt and almost all structures and fabrics in it, formed during the intense and pervasive *Transpressional Phase* and associated M_2 metamorphic cycle (Table 1). This phase involved progressive deformation, both through time and outwards to the orogen margin, from a *Wrench-Stage* to *Convergent-Stage*. Transpressional deformation occurred subsequent to emplacement of mega-crystic granites with 580 ± 3 to 552 ± 2 Ma minimum ages in the WKZ (Seth et al., 1998; Appendix A), and prior to late-stage granites of 530 ± 3 Ma in the Ugab Zone (Seth et al., 2000).
3. The Kaoko Belt was moderately reworked in a *Shortening Phase* that buckled the Kaoko Belt at the time that the Congo and Kalahari Cratons were undergoing high-angle N–S convergence, resulting in intense pervasive deformation within the Inland Branch of the Damara Orogen (Fig. 1). In the Northern Platform (Fig. 1), K–Ar whole-rock ages from Mulden Group shales give a deformation age of 535 ± 13 Ma (Clauer and Kroner, 1979), and syn-tectonic Pb–Zn–Cu mineralization at Tsumeb gives Pb–Pb model ages from galena of 530 ± 11 Ma (Kamona et al., 1999). These ages are coincident with the late-stage granite with 530 ± 1 Ma minimum age, emplaced syn-kinematic with the Shortening Phase in the Ugab Zone. The main tectonothermal phase in the Inland Branch is well constrained at 530–510 Ma (Miller, 1983; Jung et al., 2000), by Sm–Nd garnet ages and $^{207}Pb/^{206}Pb$ monazite ages from syn-kinematic granites and peak metamorphic metapelite assemblages (Jung et al., 2000). K–Ar whole-rock cooling ages of 499 ± 11 and 490 ± 11 Ma from the Kaoko Belt and Ugab Zone, respectively (Ahrendt et al., 1983), indicate that deformation and matrix assemblages formed prior to this, and cooling through 350 °C occurred at approximately 500–490 Ma.

5. Damara Orogeny—Transpressional Phase

5.1. Wrench-Stage

5.1.1. Wrench-Stage dominant L–S fabric

The first recognised deformation produced a regionally extensive, pervasive and intense bedding-parallel L-S fabric associated with small-scale isoclinal folds throughout the WKZ, CKZ and EKZ. This earliest and also most pervasive and intense expression of the Damara Orogeny almost totally reworked basement, resulting in identical structures in both basement and cover in the CKZ and WKZ. The dominant foliation is defined by bedding-parallel schistosity in the EKZ, schistose alignment of micas and quartz ± feldspar aggregate ribbons in both the CKZ and low-grade WKZ, and aligned micas and ductile grain-refined foliation ranging from proto-mylonitic to ultra-mylonitic in high-strain zones and throughout high-grade WKZ. The dominant foliation strikes NNW–SSE and is westerly inclined in almost all domains (Fig. 7) across the Kaoko Belt, being steep (60–90°) in the WKZ, moderate (40–60°) in the western CKZ and shallow (20–40°) in the eastern CKZ (Figs. 8 and 9). Only in the eastern most WKZ, adjacent to the sub-vertical PMZ, is the dominant foliation steeply inclined to the east (Figs. 2 and 6).

The dominant stretching lineation is penetrative, regionally pervasive and interpreted to represent the principal relative transport vector (Shackleton and Ries, 1984) throughout the Wrench-Stage. Dominant stretching lineation is defined by mineral aggregate ribbons of quartz and feldspar sub-grains, trains of fine micas and aligned mica, sillimanite and amphibole laths. The dominant stretching

lineation is parallel to the long axes of highly stretched clasts in diamictites and conglomerates and thus represents the *X*-axis of the strain ellipsoid. Stretching lineation orientation is very constant and plunges shallowly (0–30°) to the NNW (and less commonly SSE), parallel to the belt, throughout the WKZ and the western CKZ (Figs. 8 and 9). In the eastern CKZ stretching lineations define a spread of increasing obliquity to the orogen, ranging from NNW- to W-plunges (Fig. 8). In the steeply inclined strike-slip core of the orogen (WKZ), stretching lineations are sub-horizontal and parallel to the orogen and in the shallowly inclined foreland margin of the orogen (CKZ), stretching lineations range from oblique to down-dip orientations. This almost 90° swing in stretching lineation orientation is well illustrated on map-scale (Figs. 1 and 3–6). Boudinage of early veins and compositional layering is very common in the Kaoko Belt and the majority formed during layer-parallel shear, with flattening, associated with formation of the dominant L–S fabric (Goscombe and Passchier, 2002). Boudins are enveloped by the dominant foliation and the extension axis of boudinage is sub-parallel to the stretching lineation in the host (Goscombe and Passchier, 2002).

Shear sense in the dominant fabric has been determined, throughout the Kaoko Belt (Figs. 3, 5 and 6), using the following methods: C- and C′-type shear band cleavages (Lister and Snoke, 1984; Simpson, 1984), σ- and δ-type asymmetric mantled porphyroclasts (Passchier and Simpson, 1986), flanking folds (Hudleston, 1989; Passchier, 2001) and trains of asymmetric boudins (Goscombe and Passchier, 2002). Results are considered reliable because two or more independent methods were employed at each locality. Shear sense is consistently sinistral along shallow lineations throughout the WKZ and CKZ; this is top-to-the-SSE in the predominantly westerly inclined foliation and top-to-the-NNE where inclined to the east (Figs. 3, 5 and 6). Dextral shear sense is documented only in very few localities in the eastern over-turned limb of the Gap Antiform and Omapungwe Synform (Figs. 5 and 7). Shear sense inversion at these localities is due to refolding of the dominant fabric and associated shear sense indicators, around fold axes sub-parallel to the early stretching lineation as described by Goscombe and Trouw (1998). This simplistic model of mechanical refolding of fabrics without modification predicts that shear sense inversion should occur on all overturned limbs in terranes with co-linear late fold axes and early stretching lineations (Goscombe and Trouw, 1998), such as the Kaoko Belt. Inverted shear sense (i.e. dextral) is not universally observed on all overturned limbs of map-scale Convergent-Stage folds (Fig. 5), suggesting that the dominant fabric was reworked by progressive sinistral shear throughout the entire Transpressional Phase, including during map-scale Convergent-Stage folding.

The progressive reworking and evolution of the dominant L–S fabric during the Transpressional Phase, as implied by the regionally homogeneous sense of shear, is also supported by other observations. A continuous spread in stretching lineation orientation is apparent in all structural domains (Figs. 8 and 9), implying development of the L–S fabric throughout a protracted period of increasing obliquity of transport. Spatial partitioning of the components of transpressional strain such as strike-slip and dip-slip components (Dewey et al., 1998), would produce bimodal datasets, less continuous than those developed in the Kaoko Belt (Figs. 8 and 9). The same relationship is documented on individual outcrop scale, where lineations with different angles of obliquity are developed on different surfaces in the dominant foliation. Similar relationships have been described by Ebert and Hasui (1998) from transpressional belts in Brazil. Some outcrops preserve a refolded dominant fabric with an equally intense axial planar foliation that is co-planar with the pervasive foliation. The pervasive dominant fabric now observed in the Kaoko Belt, formed over a protracted period by continual reworking of the principal form surfaces, and is thus the accumulative sum of a history of progressive sub-parallel fabric development.

5.1.2. Wrench-Stage folding

The majority of Wrench-Stage strain was accommodated by layer-parallel shear and fabric development. Folding on any scale during this stage was not common. The earliest folds are small-scale (1–20 cm wavelength) rootless, isoclines with strong axial planar foliations and axes always parallel to the stretching lineation, plunging shallowly NNW (Figs. 8 and 9). Uncommonly, early isoclines have variable orientation in individual outcrops and have curved hinge lines with sheath like form (Figs. 5 and 6). The colinearity of fold axes and stretching lineations is common at high strains and variably interpreted to be due to hinge migration (Harland, 1971; Berthe and Brun, 1980; Cobbold and Quinquis, 1980) or folds initially forming at low angles to the stretching lineation due to differential shear (Ellis, 1986; Holdsworth and Strachan, 1991; Tikoff and Peterson, 1998).

A spectrum of fold geometries formed progressively throughout the Wrench-Stage. Second generation folds are uncommon. These are asymmetric, tight, small-scale (5–30 cm wavelength) folds that refold the dominant L–S fabric and develop either a spaced axial planar crenulation cleavage or biotite foliation. Two distinct geometries are recognised. (1) Early formed folds have axes highly oblique to the early isoclines and stretching lineations. These plunge down dip to the W in the western CKZ and to the SW in the eastern CKZ (Fig. 8). All of these ‘down-dip’ folds have sinistral fold vergence consistent with sinistral shear of the dominant foliation surface. (2) Later small-scale folds were locally developed in the western CKZ and plunge shallowly north, sub-parallel to the stretching lineation (Fig. 8). These have W over E fold vergence on both limbs of large-scale Convergent-Stage overturned folds, also of W over E vergence, indicating that they were refolded and not parasitic to these large-scale folds. These indicate that the

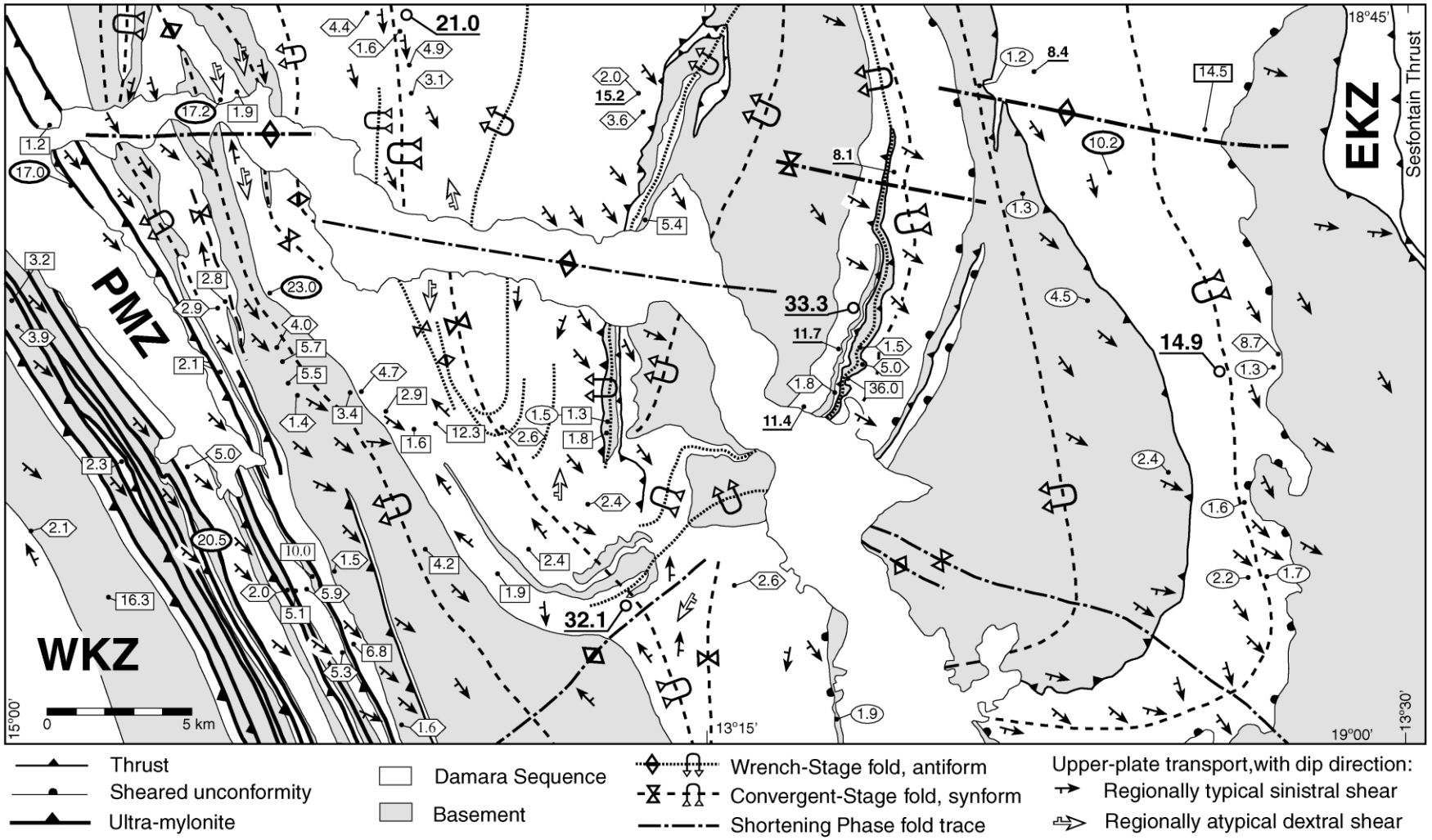

Fig. 5. Structural map of the CKZ portion of the central profile, with Wrench-Stage strain estimates (Appendix B) indicated. Strain ratio (R) is calculated from extension of drawn and shearband boudins (hexagons and squares respectively) after Goscombe and Passchier (2002), quartz fringes on magnetite (bold square) and average aspect ratio of clasts in conglomerates and diamictites (underlined). Localities with clasts indicating constrictional strains (Fig. 11) are highlighted by open circles and large font. Shear strain (γ) is calculated from the angle between C′- and S-planes (ellipses) after Ramsay and Graham (1970) and sheath fold geometry (bold ellipses) after Lacassin and Mattauer (1985). All ultramylonite (>90% grain-refinement) and mylonite shear zones are indicated. Direction of closure and the dip of limbs of major overturned synforms and antiforms are indicated by arrow symbols.

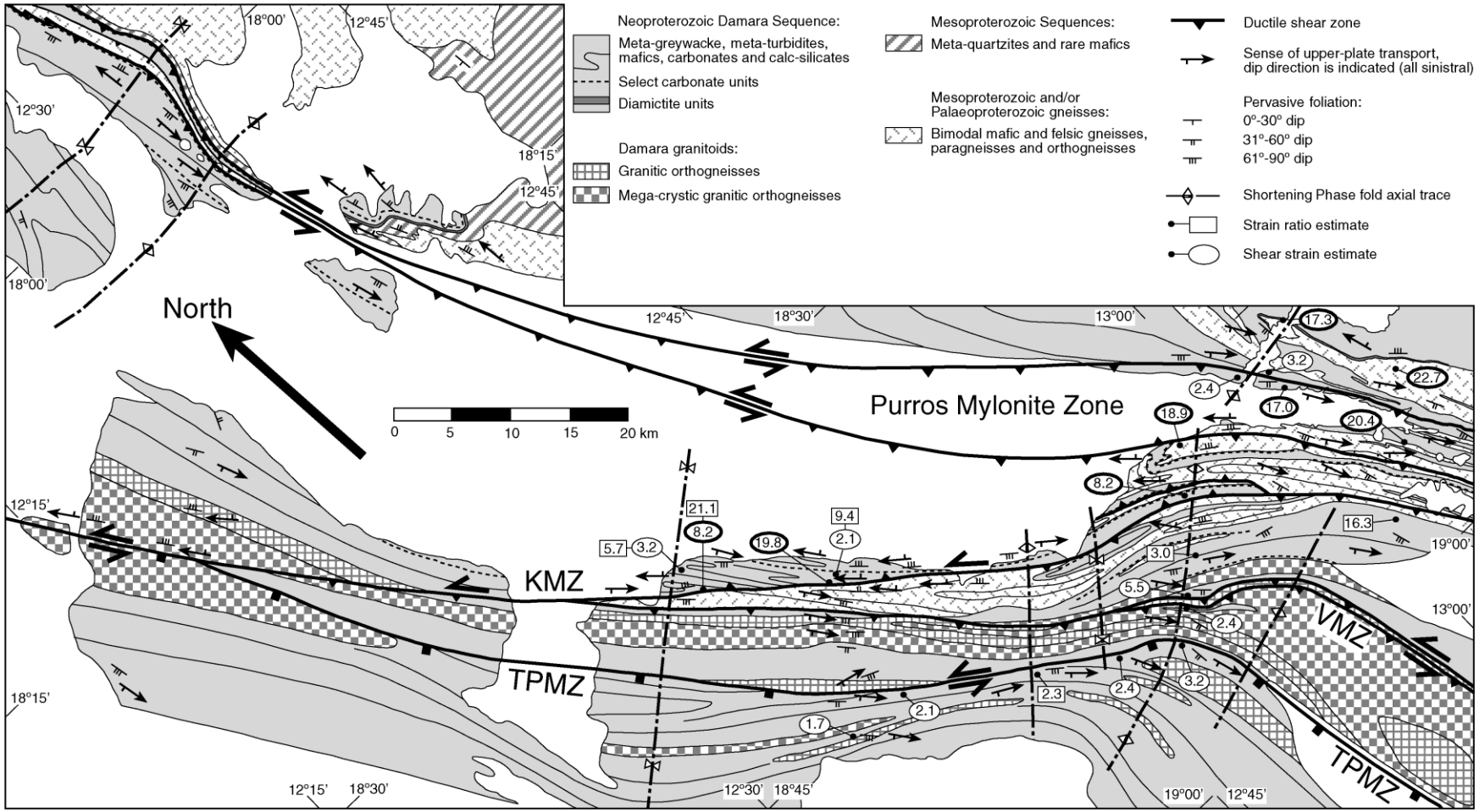

Fig. 6. Structural and chrono-stratigraphic map of a portion of the WKZ mapped in detail, with major structures named and Wrench-Stage strain estimates (Appendix B) indicated. Strain ratio (R) and shear strain (γ) are calculated and labelled as in Fig. 5. Shear zones labelled as in Fig. 2. Convergent-Stage fold axial traces are sub-parallel to the structural grain but not indicated for clarity.

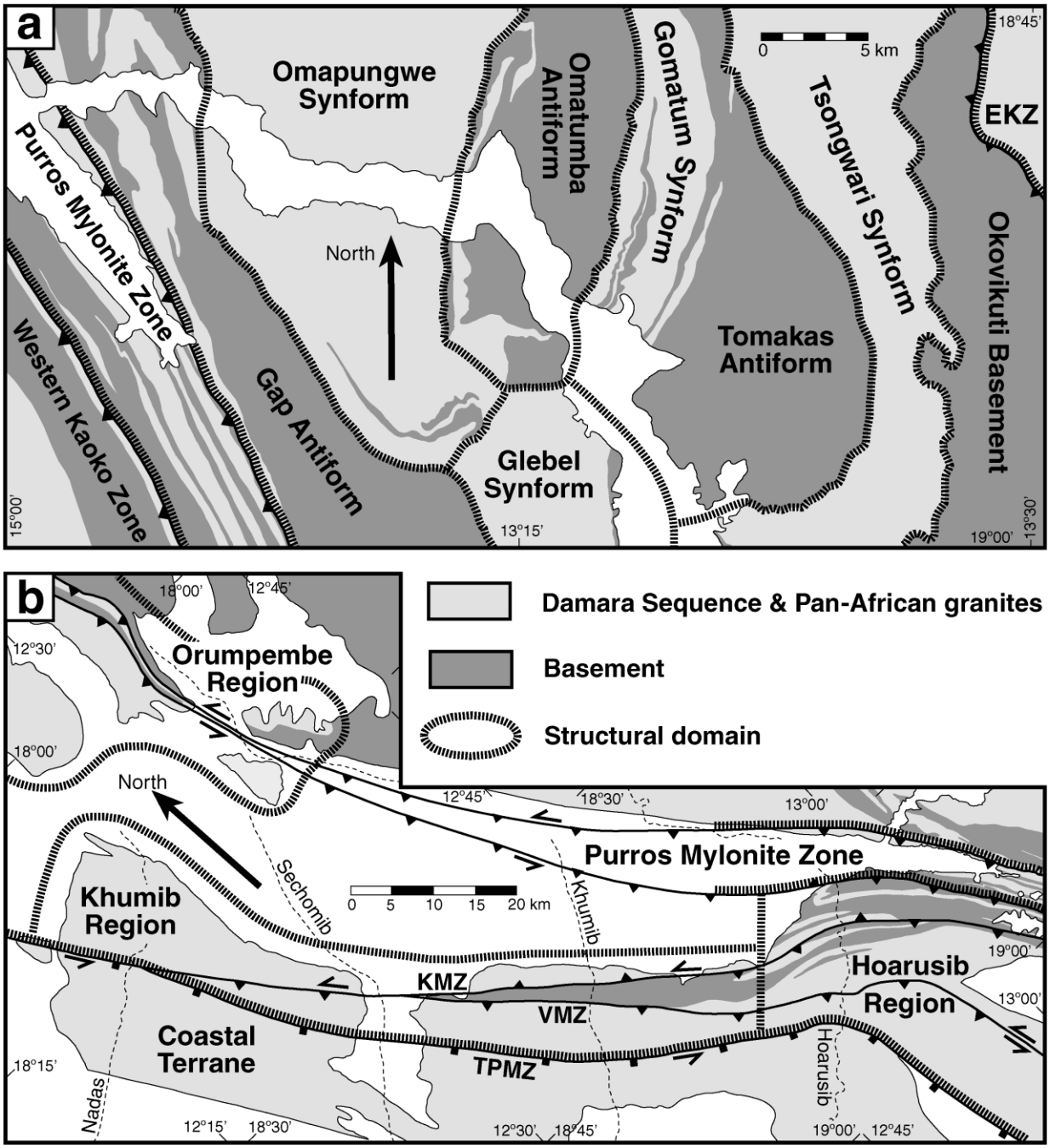

Fig. 7. Names of major structures and outline of structural domains referred to in Figs. 8 and 9. (a) Area outlined in Fig. 5. (b) Area outlined in Fig. 6.

earliest expression of W over E transport gave rise to small-scale folding of the dominant foliation surface immediately prior to large-scale W over E transport in the Convergent-Stage.

5.1.3. Wrench-Stage shear zones in the WKZ

The WKZ is dissected into NNW-trending laterally extensive panels of rock, by a network of crustal-scale, sub-parallel, steep, sinistral ductile shear zones. The eastern margin of the WKZ was originally defined as the Purros Lineament (Miller, 1983). Our mapping has established this margin to be a steep 4.5-km-wide shear zone consisting almost entirely of mylonite and ultra-mylonite (Goscombe, 1999d) which we have renamed the Purros Mylonite Zone (PMZ) (Goscombe, 1998; Goscombe and Hand, 2001). To the west, the Khumib Mylonite Zone is a sub-vertical network of at least two mylonite zones each at least 10 m wide, in the high-grade core (Hoarusib Region) of the WKZ (Fig. 6). Along strike to the north, the Khumib Mylonite Zone is a single 20-m-wide mylonite and ultramylonite zone with numerous sheath folds, that juxtaposes low-grade Damara Sequence against basement gneisses (Figs. 2 and 6).

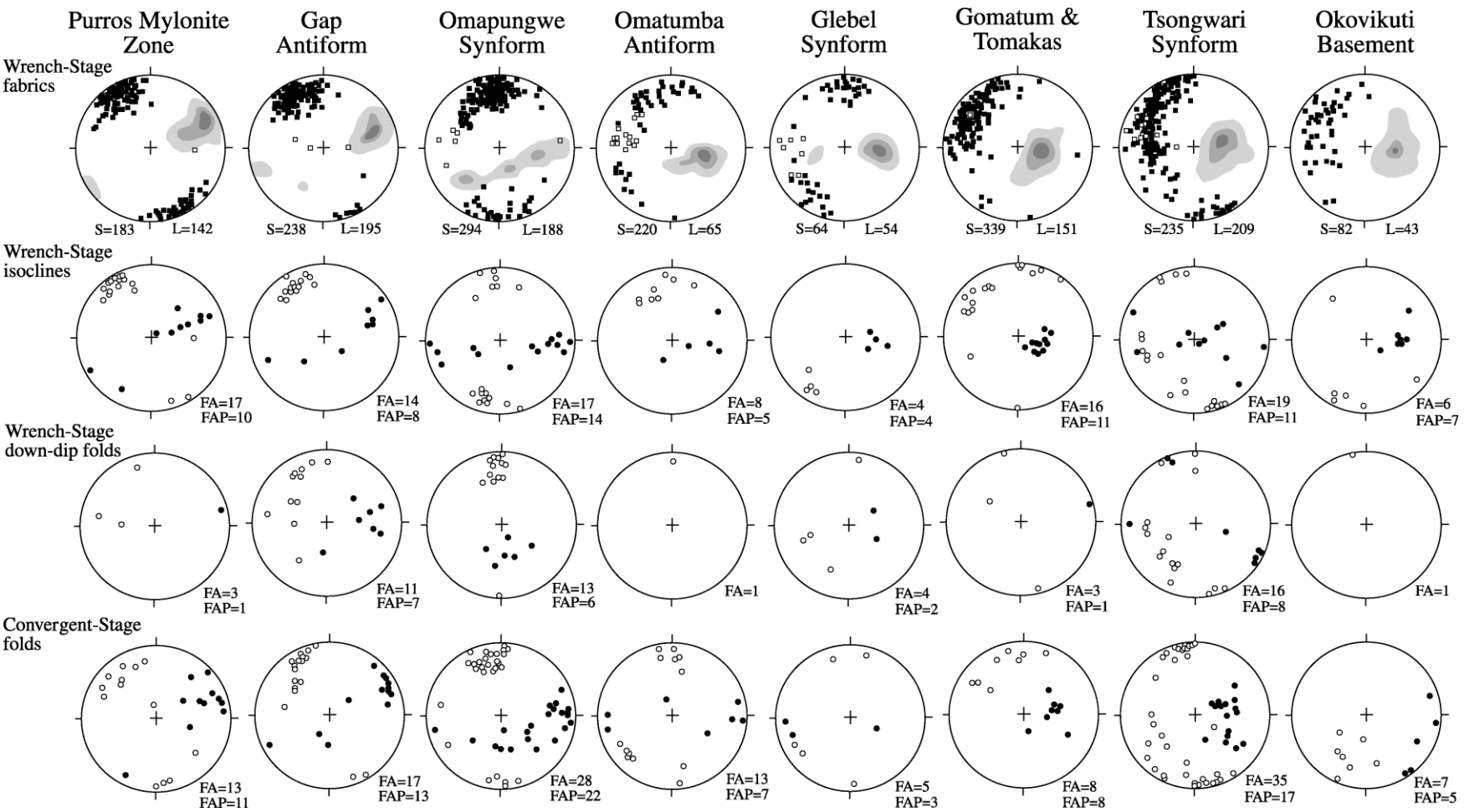

Fig. 8. Lower-hemisphere, equal-angle stereoplots of Transpressional Phase structures in domains from west to east across the CKZ in the area mapped in detail (Fig. 5). Time progresses down the page. Solid squares—dominant mineral aggregate stretching lineation; open squares—aligned mineral lineation; contoured region—poles to dominant foliation; open circles—plunge of fold axes; solid circles—poles to fold axial planes. Contours at three, six and nine times uniform distribution of data.

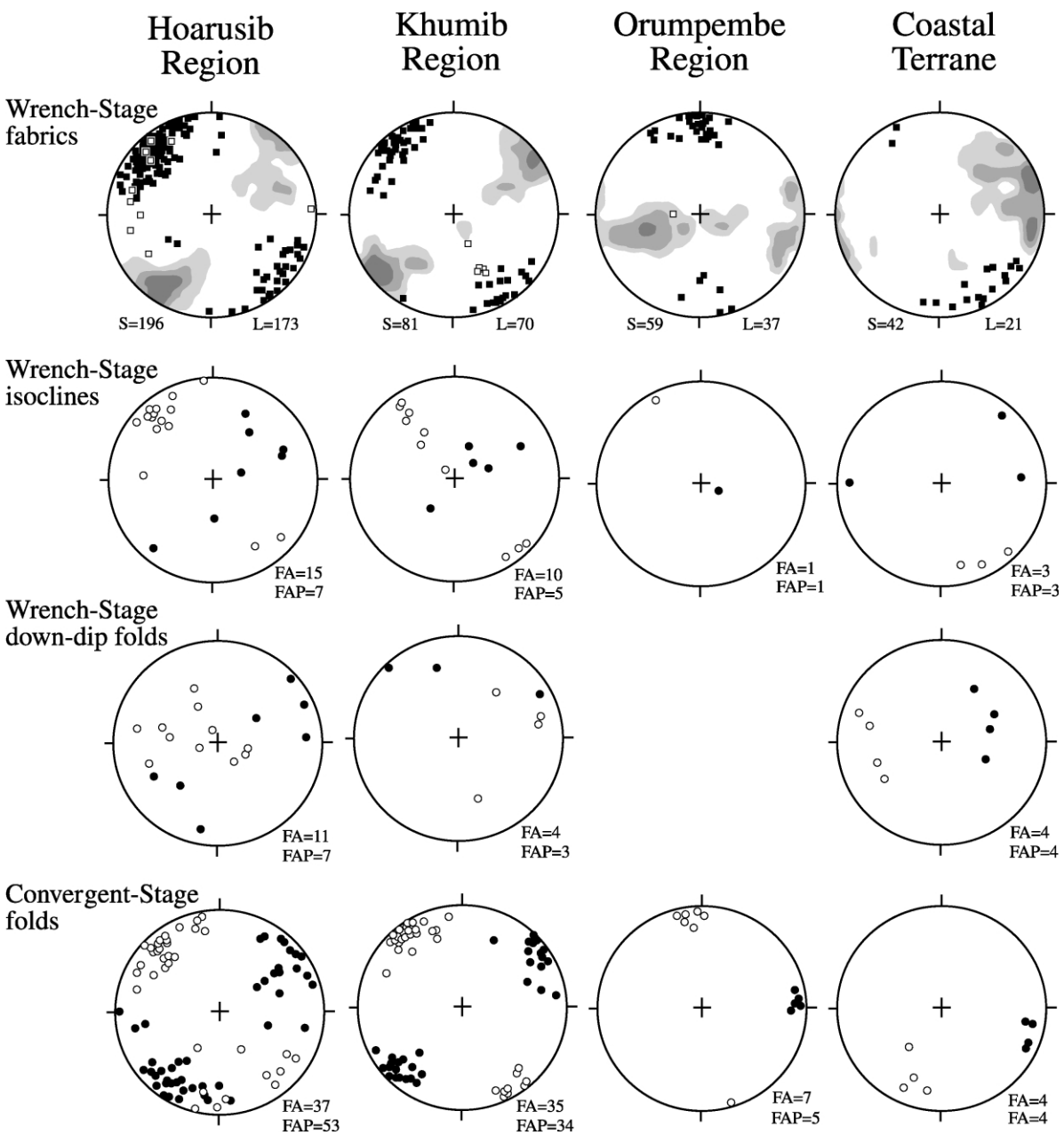

Fig. 9. Lower-hemisphere, equal-angle stereoplots of Transpressional Phase structures in domains from the WKZ (Fig. 6). Time progresses down the page. Solid squares—dominant mineral aggregate stretching lineation; open squares—aligned mineral lineation; contoured region—poles to dominant foliation; open circles—plunge of fold axes; solid circles—poles to fold axial planes. Contours at three, six and nine times uniform distribution of data.

To the west two further mylonite zones are inclined 60° to the west and each juxtaposes Damara Sequence and Pan-African granite gneisses of successively lower-grade towards the west (Figs. 2 and 6). The first of these, the Village Mylonite Zone, is a network of mylonites 1 km wide, at the margin of a panel dominated by Pan-African granites. The western-most, Three Palms Mylonite Zone, is a poorly exposed $>$100-m-wide mylonite and ultramylonite zone. Some of these shear zones may be terrane boundaries. The PMZ is possibly the boundary between Palaeoproterozoic and Mesoproterozoic basements, and the Three Palms Mylonite Zone is the east margin of the Coastal Terrane (Fig. 6), a distinctly different Damara Sequence of massive greywackes devoid of mafics and carbonates.

The PMZ is a crustal-scale, orogen median, ductile shear zone that can be traced for at least 500 km. Characterized by extremely high shear strains ($\gamma > 10$; Fig. 6) that imply lateral displacement $\gg$ 50 km. The PMZ controlled the architecture of the entire Kaoko Belt and remained active throughout the whole Transpressional Phase, from early in the Wrench-Stage to being the root zone of outward vergent over-folds and nappes in the Convergence-Stage (Fig. 2). In the central Kaoko Belt region detailed mapping (Figs. 5 and 6) shows the PMZ to be a 4.5-km-wide mylonite zone,

bounded sharply by ultramylonite zones, and containing a further nine ultramylonite zones, each of 50–100 m in width. The PMZ is dominated by an intense L–S fabric with little folding, though sheath folds are documented (Figs. 5 and 6). The orientation of the PMZ and the mylonitic L–S fabric within it, are parallel to and continuous into the dominant fabric either in the adjacent WKZ or CKZ. Mylonites are comprised of statically annealed quartz and feldspar polygonal granoblastic aggregate ribbons, indicating the thermal peak and annealing subsequent to shearing. Ultramylonites consist of >90% matrix of very fine glass-like aggregate ribbons with contorted flow folds and isolated, rounded porphyroclasts of feldspar, quartz and hornblende.

To the south, the eastern bounding ultramylonite of the PMZ is directly along strike from a 100-m-wide, westerly inclined (50°) ultramylonite zone in the Hoanib traverse that marks the eastern boundary of mylonites in the WKZ and Mesoproterozoic basement dated by Seth et al. (1998). Further south the PMZ is interpreted to continue along strike to the Ogden Mylonite Zone at the western margin of the Ugab Zone (Fig. 10; Freyer and Halbich, 1994; Hoffman et al., 1994). The Ogden Mylonite Zone dips steeply (70°) east, experienced sinistral shear along shallow NNW-plunging lineations and grain-refined partially melted greywackes of the Damara Sequence. To the north in the Orumpembe Region (Fig. 7), the PMZ is a 2-km-wide, steeply (60–70°) west-dipping shear zone containing slivers of basement and mylonitized Damara Sequence carbonate and quartzite units and juxtaposes basement against low-grade Damara Sequence in the west (Fig. 6). The PMZ can be traced northwards into Angola as a prominent sinistral shear zone on Landsat images, juxtaposing basement exposures in the CKZ with Damara Sequence and Pan-African granites in the WKZ (Fig. 3). Along the entire length of the PMZ, shear sense is consistently sinistral and obliquely reverse along shallow NNW-plunging stretching lineations.

5.1.4. Wrench-Stage bulk strain and flow regime

Pervasive and intense foliations and stretching lineations suggest high bulk shear strains were experienced throughout the whole WKZ and CKZ during the Wrench-Stage. Semi-quantitative measurements of strain intensity were made by a variety of methods (Appendix B), calculated as strain ratio (R) assuming plane strain and shear strain (γ) assuming simple shear. These are represented spatially across the Kaoko Belt (Figs. 5 and 6). Elongation of quartz fibre fringes on magnetite grains (Ramsay and Huber, 1983), parallel to the stretching lineation in matrix quartz–sericite schist, give an average strain ratio of 14.5 (Fig. 5). Stretch of the enveloping surface to boudin trains (Goscombe and Passchier, 2002) are typically moderate but give strain ratios up to 36.0 and 23.8 in drawn and shearband boudins, respectively (Figs. 5 and 6). Aspect ratios of stretched clasts in conglomerate and diamictite units give minimum estimates of bulk strain (Appendix B; Figs. 5 and 6). The principal extension axis (X) is parallel to the long axes of clasts and is sub-parallel to the stretching lineation in the matrix, whereas the Z-axis is orthogonal to the foliation (containing the X- and Y-axes). The average strain ratio from each locality ranges from 8.1 to 33.3 (Fig. 5) and shear strain calculated after the method of Ramsay (1967), assuming simple shear, ranges from 2.5 to 5.5 (Appendix B). In these rocks, bulk strain calculations can only be considered minimum estimates because strain is differentially partitioned between matrix and clast. At opposite ends of the spectrum, granite clasts give the lowest estimates and carbonate clasts give estimates closest to the bulk strain experienced because clast and host are of similar competence.

Angular relationship between shear bands and the pervasive foliation (θ) is related to shear strain (γ) by the relationship $\gamma = 2/(\tan(2\theta))$ (Ramsay and Graham, 1970). In the area mapped, θ ranges from 11 to 35° and calculated shear strain ranges from 0.73 to 4.95 with an average γ of 2.19 (Appendix B). Schists and mylonites with C′-shear bands are regionally pervasive and mylonites with coplanar S–C foliations are common, both indicating shear strains >2.3 (Burg and Laurent, 1978; Berthe et al., 1979; Ramsay, 1979). Co-linearity of stretching lineations and early fold axes attests to the high shear strains ($\gamma > 10$) during the Wrench-Stage (Berthe and Brun, 1980; Cobbold and Quinquis, 1980). Sheath folds with long axes parallel to the stretching lineation are rare in the CKZ and common in the PMZ and crustal-scale shear zones of the WKZ. Shear strain estimates from sheath fold geometry using the method of Lacassin and Mattauer (1985) ranges from 3.7 to 22.7 with an average of 13.3 (Fig. 6). These calculated shear strains are considered realistic estimates of the bulk strain experienced by the rock volume. In contrast, most other methods are minimum estimates, where to varying degrees a proportion of strain is not recorded because strain is preferentially partitioned into the enveloping ductile foliation and not the competent boudins, cobble clasts and porphyroclasts employed for strain calculations.

These semi-quantitative strain measurements indicate that bulk strain during development of the dominant L–S fabric was on the whole high ($\gamma = 2–10$) across the CKZ and WKZ (Figs. 5 and 6). Superimposed on this regionally pervasive high bulk strain are discrete thrusts and shear zones, with mylonitic to ultramylonitic fabrics, which are interpreted to have experienced much higher bulk strain (γ up to 23) than background values. In the CKZ most of these high strain zones are in the vicinity of the contact between basement and Damara Sequence (Fig. 5). Bulk strain in the PMZ and other crustal-scale shear zones in the WKZ, was significantly higher than background strain in the CKZ and the panels of rock between these shear zones. In these shear zones, mylonite and ultramylonite fabrics experienced 75–90% and >90% ductile grain-refinement, respectively, to fine (0.01–0.2 mm) sub-grain aggregate ribbons and highly

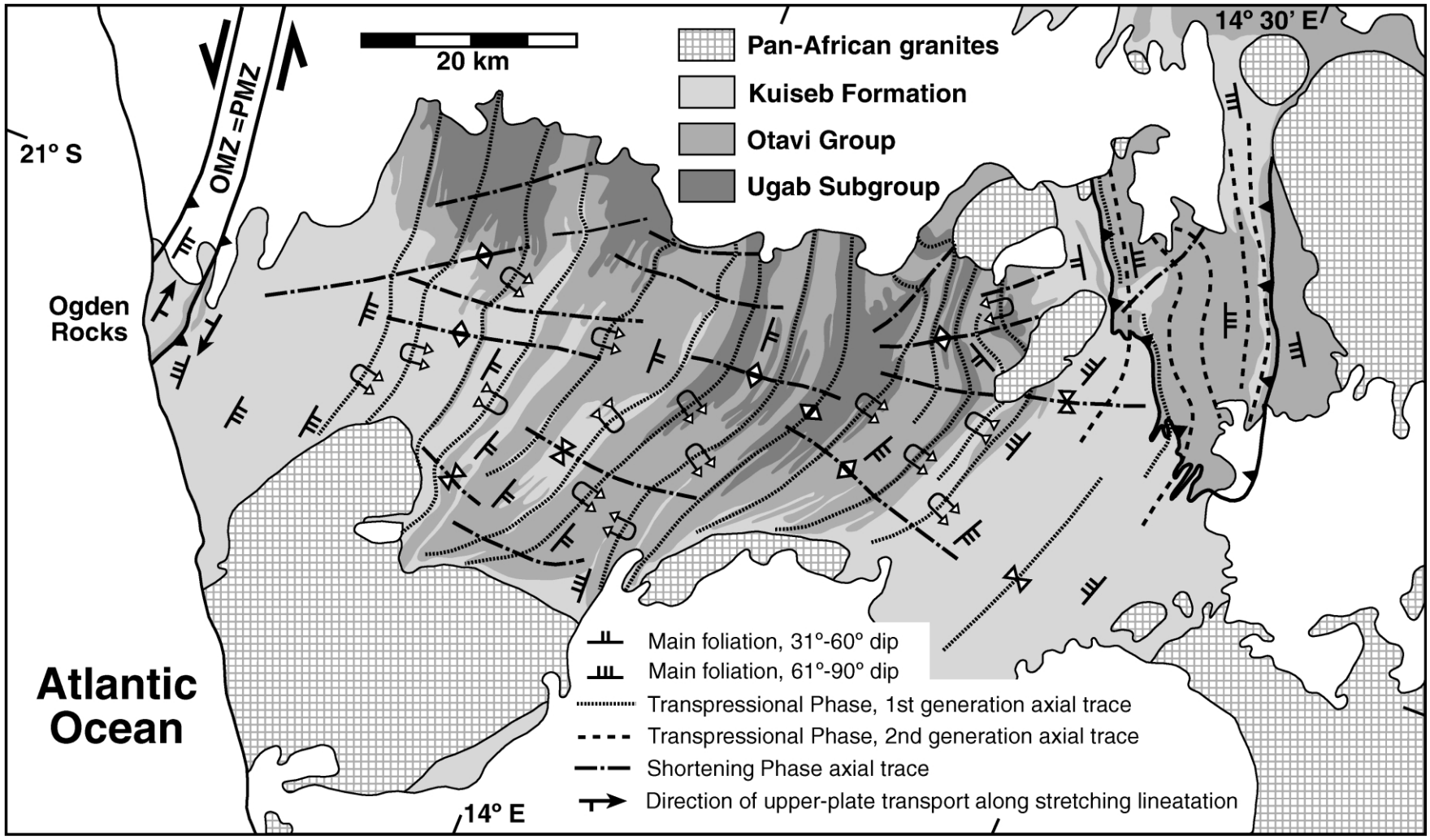

Fig. 10. Simplified map of the Ugab Zone (southern-most Kaoko Belt) indicating the major chrono-stratigraphic rock units. Dip of the pervasive axial planar foliation is indicated. For clarity, only select Transpression Phase folds are indicated and their vergence illustrated by the overturned synform and antiform symbols (Fig. 5). Stretching lineations are rare in the Ugab Zone, upper-plate transport direction at these localities are indicated using the same symbol as in Fig. 3. Map sourced from Miller and Grote (1988), Hoffman et al. (1994) and the authors work. OMZ—Ogden Mylonite Zone, the southern lateral extension of the PMZ.

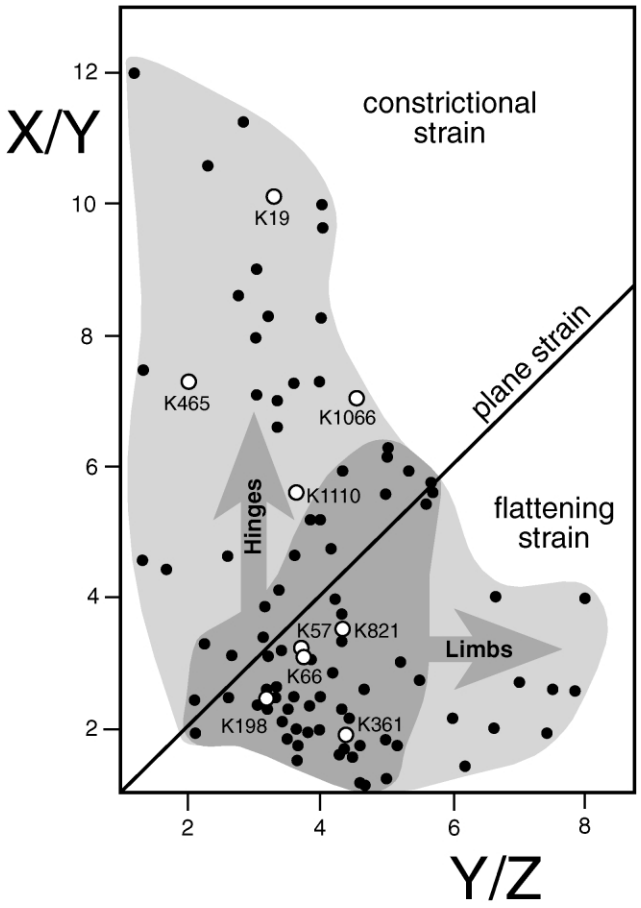

Fig. 11. Flynn diagram of clast aspect ratios from deformed conglomerate and diamictite localities. Solid dots are individual clasts and open circles are averages representing a specific locality (Appendix B). Dark shading—majority of the data, represents typical Wrench-Stage strain. Pale shading—field of extreme clast shapes, possibly modified by reworking in the Convergence-Stage (see text).

elongate sheath folds are common, documenting shear strains of up to 23 (Fig. 6).

The Wrench-Stage pervasive L–S fabric formed in a non-coaxial shear environment. Non-coaxial shear is indicated by the colinearity of fold axes and stretching lineations, sheath folds (Berthe and Brun, 1980; Cobbold and Quinquis, 1980), regionally consistent sinistral sense of shear and pronounced monoclinic asymmetry of developed structures (composite foliations, boudins, mantled porphyroclasts and asymmetric folds). These features indicate that pure shear did not dominate in the Wrench-Stage when the L–S fabric was forming. In contrast, Convergent-Stage structures in the CKZ and WKZ (nappes, asymmetric overfolds, tight upright folds, crenulations and thrusts) also indicate an overall non-coaxial shear environment, but with a significant component of pure shear. This evolution towards more flattening strains in the Convergent-Stage is illustrated by the aspect ratios of stretched clasts in conglomerates and diamictites. Plotted in a Flynn diagram, the clast data outlines a large continuous spread from flattening to constrictional strains, with most data clustering around plane strain and into the flattening field (Fig. 11). The highly constrictional and highly flattening strains recorded are the result of further modification of clast shapes during Convergent-Stage reworking. Apparent constrictional strains are documented in only four localities; all of these occur in the hinge zones of large-scale Convergent-Stage synforms (Fig. 5). In hinge zones, the Wrench-Stage *Y*-axis of the deformed clasts was closely aligned with the Convergence-Stage *Z*-axis, and shortening along this axis produced modified prolate clast shapes (Fig. 11). Localities on the limbs of Convergent-Stage folds experienced further shortening along an axis similar to the earlier *Z*-axis, further enhancing oblate clasts shapes and enlarging the flattening strain field (Fig. 11).

5.1.5. Basement/cover relationships

Basement/cover relationships differ significantly across the belt. In the high-grade internal part of orogen (WKZ and CKZ) basement and cover rocks are deformed similarly. Only in the foreland (EKZ) is a distinct contrast in deformation style developed; between weakly reworked coarse gneissic basement and strongly foliated Damara Sequence. Nevertheless, the unconformity was rarely reactivated as a high-strain shear discontinuity during the Damara Orogeny. The eastern-most basement/cover contact in the CKZ (i.e. eastern limb of the Tsongwari synform; Fig. 5) preserves its unconformable nature regionally throughout the Kaoko Belt, including discontinuous granite gravel regolith. Westward throughout the CKZ and WKZ, the basement/cover contact can be considered a ductilely sheared unconformity, with similar strain intensity at the unconformity surface as throughout the adjacent basement and cover rock masses. Reworking of basement was intense and the regionally pervasive L–S fabric is developed throughout (Fig. 5), indicating that deformation of basement and cover was linked and the unconformity did not operate as a strain discontinuity. This resulted in both basement and cover in the CKZ and WKZ being similarly deformed throughout the Damara Orogeny and the unconformity being folded in the Convergent-Stage. High-strain shear zones and thrusts slivers at, or in the vicinity of, the basement/cover unconformity have been recognised within the Gomatum Synform and western margin of the Omatumba Antiform, but are not characteristic of this contact (Figs. 2, 5 and 6).

5.2. Convergent-Stage

5.2.1. Convergent-Stage folds

Map-scale (kilometre-scale wavelength), shallow-plunging, inclined, east vergent nappe and asymmetric folds dominate the structure of the Kaoko Belt (Figs. 5 and 12), and are characteristic of the Convergent-Stage of deformation late in the Transpressional Phase. Both map-scale nappes and associated parasitic mesoscopic folds are asymmetric, tight to isoclinal, ‘similar’ folds with curved

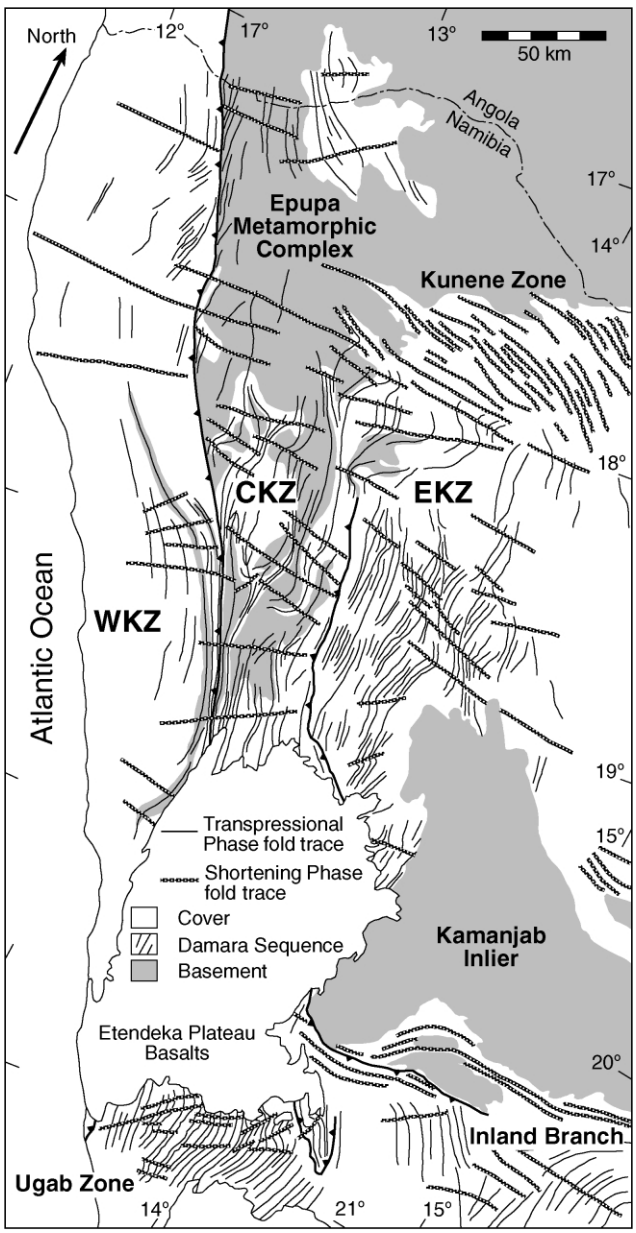

Fig. 12. Simplified map of the axial trace of major folds throughout the entire Kaoko Belt in Namibia. Tight to isoclinal folds from the Transpressional Phase are distinguished from late-stage, upright open to close Shortening Phase folds. Data sourced from authors work, unpublished maps and literature.

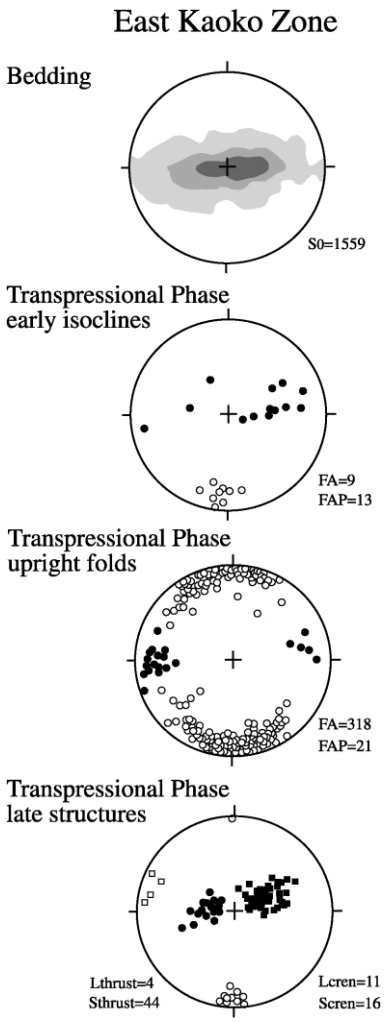

Fig. 13. Lower-hemisphere, equal-angle stereoplots of deformation structures in the EKZ (Fig. 12). Data sourced from authors work, unpublished maps and literature, principally Guj (1970). Solid squares—poles to thrusts; open squares—stretching lineations; contoured region—poles to bedding; open circles—plunge of fold axes; solid circles—poles to fold axial planes. Contours at three, six and nine times uniform distribution of data.

hinges that refold early isoclines, drag folds and the pervasive L–S fabric. Convergent-Stage folds have shallow (0–30°) plunges to the N to NW and SW (Figs. 8, 9 and 13), are co-linear to the Wrench-Stage isoclines (Figs. 8 and 9) and the belt in general. As such they are typical of transpressional belts (Harland, 1971; Haq and Davis, 1997; Tikoff and Peterson, 1998). Convergent-Stage folds display a trend across the belt from NW-plunges in the WKZ (Fig. 9), N-plunges in the western CKZ, N- and SW-plunges in the eastern CKZ (Fig. 8) and horizontal to S-plunges in the EKZ (Fig. 13). Similarly, fold inclination varies systematically across the Kaoko Belt, defining a gross architecture of a steeply divergent flower structure in the core of the orogen. This is centred on the PMZ, with progessively shallower, west-inclined and east-vergent nappes in the eastern CKZ (Fig. 2). Convergent-Stage folds are inclined 60–80° west in the Coastal Terrane, inclined 60–90° to both the east and west in the eastern WKZ (Fig. 9), ranging from 40–80° to 20–50° westerly inclination across the CKZ (Fig. 8) and sub-vertical (60–90°) with both east and west inclination in the EKZ (Fig. 13).

Convergent-Stage folds in the high-grade WKZ develop a weak axial planar mica foliation and uncommonly have thin (0.5–3 cm) axial planar partial melt segregations, but are otherwise too coarse-grained to develop crenulation cleavages. In the CKZ, a new axial planar schistosity was not developed but crenulation cleavages are common. Discrete crenulation cleavages are developed only where

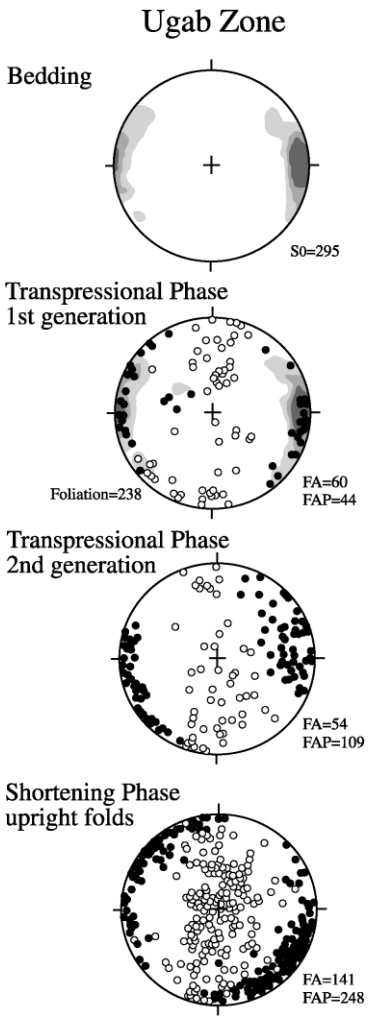

Fig. 14. Lower-hemisphere, equal-angle stereoplots of deformation structures in the Ugab Zone (Fig. 10). Data sourced from authors work. Contoured regions—poles to bedding or pervasive foliation; open circles—plunge of fold axes; solid circles—poles to fold axial planes. Contours at three, six and nine times uniform distribution of data.

axial surfaces are sufficiently oblique to the early schistosic foliation. A wide range in orientation of weak, spaced crenulation cleavages formed as progressive folding rotated the dominant foliation through the stress field and into orientations conducive to crenulation (Fig. 8). Crenulation lineations are sub-parallel to all scales of Convergent-Stage folds and earlier formed stretching lineations and isoclines (Figs. 8, 9 and 13). In the low-grade WKZ, the tight to isoclinal Convergence-Stage folds have spaced axial planar foliation seams at a low-angle to the early schistosity. These seams have shear band-like geometries and display consistently sinistral shear sense, indicating that Convergent-Stage folding in the WKZ accompanied sinistral transpressional strain.

Convergent-Stage folds in the CKZ and WKZ are interpreted to have formed in a non-coaxial shear environment, as indicated by their consistent asymmetry in the profile plane and formation of crenulation cleavages with sinistral shear band geometries. These folds are moderately to steeply inclined, have axes normal to the inferred transport direction (see below) and consistent fold asymmetry vergence and nappe style indicate both significant dip-slip non-coaxial shear and flattening strains. In contrast, Convergent-Stage folding in the EKZ formed by pure shear shortening, producing kilometre-scale wavelength, upright and symmetric cylindrical folds with sub-vertical crenulation cleavages and horizontal N–S axes (Fig. 13). The Ugab Zone is dominated by two heterogeneously partitioned generations of colinear and horizontal, tight and asymmetric map-scale folds that are typically steeply inclined and verge both to the east and west (Figs. 1, 10 and 14; Coward, 1981; Weber and Ahrendt, 1983; Hoffman et al., 1994). These N–S-trending folds formed without involvement of basement, during NW–SE transpression and E–W shortening in the Convergent-Stage (Freyer and Halbich, 1994).

Mineral lineations defined by aligned coarse-grained hornblende and biotite laths are sparsely developed throughout the CKZ and WKZ. Where developed, these mineral lineations post-date the strong mineral aggregate stretching lineation and plunge down-dip to the W to WNW. Wrench-Stage mineral aggregate lineations and Convergent-Stage aligned mineral laths overlap in orientation (Figs. 6 and 8), indicating progressive deformation through both stages of the Transpressional Phase. Aligned mineral laths are the latest-formed, texturally recognizable end-member in the progressive development of stretching lineations, evolving from sub-horizontal to higher angles of obliquity through the Wrench-Stage and into the Convergent-Stage (Figs. 8 and 9). Aligned mineral lath lineations are developed at high angles to the axes of Convergent-Stage folds and represent the axis of maximum extension at this stage. Consequently, the aligned mineral laths define the vector of tectonic transport during west-over-east transport and development of nappe folds during high-angle convergence across the Kaoko Belt late in the sinistral Transpressional Phase.

Tectonic transport in the Convergent-Stage, was approximately orthogonal to the orogen-parallel stretching lineations in the Wrench-Stage. These two end-member strain states are recorded both by stretching lineation populations (see above) and by boudin train geometries. The vast majority of boudins developed in the Kaoko Belt (88%) have extension axes (orthogonal to the boudin long axis within the enveloping foliation; Goscombe and Passchier, 2002) sub-parallel to the Wrench-Stage stretching lineations, and formed during development of the dominant fabric. A distinct boudin sub-population (12%) has extension axes orthogonal to the Wrench-Stage boudins and sub-parallel to the inferred E–W-trending Convergent-Stage transport direction (Goscombe and Passchier, 2002). These formed in two distinct structural settings; as foliation-parallel boudin trains on the long limbs of asymmetric folds and as foliation-oblique boudin trains in over-turned limbs. Therefore, lineation populations, fold geometries and

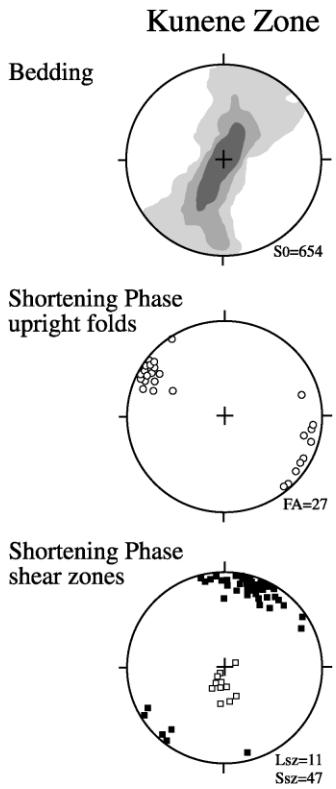

Fig. 15. Lower-hemisphere, equal-angle stereoplots of deformation structures in the Kunene Zone (Fig. 12). Data sourced from authors work and unpublished maps. Solid squares—poles to retrograde shear zones; open squares—stretching lineations; contoured region—poles to bedding; open circles—plunge of fold axes; solid circles—poles to fold axial planes. Contours at three, six and nine times uniform distribution of data.

boudin train populations all confirm that there were two temporally sequential and geometrically distinct end-member strain states bracketing the progressive Transpressional Phase of orogenesis.

5.2.2. Convergent-Stage thrusts

EKZ folds were progressively tightened into box-shaped profiles with late-stage cleavages, folds and thrusts developed, indicating progressive shortening late in the Convergent-Stage in the EKZ. The western margin of the EKZ is a network of brittle thrusts called the Sesfontain Thrust (Guj, 1970; Hoffman et al., 1994). These strike NNW, are inclined 15–45° west and have WNW-plunging slickenlines (Fig. 13) indicating high-angle oblique WNW over ESE thrusting. The eastern-most CKZ and western-most EKZ have late-formed, strongly developed shallow west-inclined crenulation cleavages, indicating that the Sesfontain Thrust formed by brittle failure late in a continuum of west-over-east ductile transport. Progressive E–W shortening of the EKZ further tightened the synclinorium of Mulden Group molasse, resulting in a broad divergent structure representing an inverted flower structure (Fig. 2). The eastern margin of this structure, developed shallow east-inclined, late-stage crenulation cleavages with east-over-west vergence (Fig. 13) and steep, east-dipping brittle thrust faults and thrust-related box-shaped hinges in the thick carbonate sequences (Hoffman et al., 1994).

6. Damara Orogeny—Shortening Phase

A later phase of deformation, entirely distinct from the Transpressional Phase, involved minor N–S shortening strain resulting in large-scale (5–50 km wavelength) upright buckling of the central Kaoko Belt (Fig. 12). These upright E-trending folds gave rise to interference patterns with oppositely plunging culminations of Convergent-Stage nappes and overfolds (Figs. 3–5). Mesoscopic Shortening Phase folds are rare and occur as upright, open to close folding of the dominant L–S fabric around typically rounded hinges of 2–1000 cm wavelength. No axial planar foliation was developed. Axial surfaces are vertical and trend ENE to ESE with axes plunging 15–55° towards the west. Despite the low-angle between the trace of pre-existing foliations and axis of N–S shortening during the Shortening Phase, kinkbands are surprisingly rare throughout the whole Kaoko Belt. Those present in the Kaoko Belt have 1–30 cm width, with steep, sinistral kinkbands trending NE and dextral kinkbands trending NW, in response to sub-horizontal N–S σ_1. In the Ugab Zone kinkbands are steep, have 1–10 cm width, with dextral kinkbands trending NW and sinistral kinkbands trending ENE, in response to sub-horizontal NNE-SSW σ_1.

Shortening Phase strain was greatest at the northeastern and southern margins of the Kaoko Belt, within the Kunene and Ugab Zones (Fig. 12), where the structures developed are significantly different to those in the central Kaoko Belt region. The dominant structures developed in the Kunene Zone (Fig. 12) and Northern Platform of the Inland Branch (Fig. 1) are kilometre-scale, upright, E- to ESE-trending tight to open cylindrical folds with horizontal axes (Figs. 12 and 15). In these regions, expressions of the earlier Transpressional Phase are insignificant. Shortening Phase folds dominate and have significantly tighter inter-limb angles and shorter wavelength, indicating higher N-tending shortening strain than experienced in the central Kaoko Belt region. Shortening Phase, greenschist facies, 20–400-m-wide retrograde shear zones are only developed in the Kunene Zone. These are tabular, have consitent ESE-trends, dip 80° south (Fig. 15) and have reverse movements along sub-vertical stretching lineations giving palaeo-stress solutions with horizontal NE–SW-trending σ_1 (Goscombe, 1999a).

Shortening Phase folds in the Ugab Zone have E- to ENE-trending, steep axial surfaces, similar to those elsewhere in the Kaoko Belt (Figs. 12 and 14; Weber and Ahrendt, 1983; Freyer and Halbich, 1994; Hoffman et al., 1994). These folds differ by having sub-vertical axes and fold asymmetry with sinistral vergence, consistent with the N–S shortening axis. Shortening Phase strain was also heterogeneously partitioned into 5-km-wide,

NE–SW-trending higher strain zones containing open to tight map-scale and mesoscopic folds with steep NE- to E-trending axial surfaces and crenulation cleavages. The aureoles of syn-tectonic granites contain a micaceous schistosity of NE-strike (Fig. 14).

The Transpressional Phase deformation regime involved non-coaxial shear and a significant lateral movement component resulting from south-directed transport of the outboard Brazilian Plate. In contrast, the Shortening Phase involved N–S shortening in a pure shear environment with little non-coaxial shear component. Change in the deformation regime was due to a reorganisation of the Damara Orogeny on crustal plate scale. Strain during the Shortening Phase was heterogeneously partitioned throughout the Kaoko Belt, with only minimal reworking in the central Kaoko Belt region but strong deformation in the Kunene Zone and Ugab Zone. At this time, the deformation front had moved to the south and east and is correlated with the main orogenic phase in the Inland Branch, resulting from high-angle convergence of the Congo and Kalahari Cratons (Fig. 1; Coward, 1983; Freyer and Halbich, 1994).

7. Discussion

7.1. Spatial and temporal progression in deformation across the Kaoko Belt

There is a continually smooth transition from orogen-parallel lineations in the orogen core to higher-angle oblique lineations on the margin of the Kaoko Belt (Figs. 3, 5 and 6). This is a feature in common with and typical of mid-crustal transpressional orogens (Shackleton and Ries, 1984; Bale and Brun, 1989; Holdsworth and Strachan, 1991; Ebert and Hasui, 1998). Continuous symmetrical partitioning (Dewey et al., 1998) with orogen-median, high-strain strike-slip shear zones such as the PMZ are also typical (Bale and Brun, 1989; Soper et al., 1992; Robin and Cruden, 1994; Tikoff and Teyssier, 1994; Camacho and McDougall, 2000) and represented by median transcurrent brittle fault systems in the upper-crust (Teyssier and Tikoff, 1998). The alternative scenarios of discontinuous strain partitioning (Dewey et al., 1998) or transpressional orogens with alternating panels of contemporaneous strike-slip versus thrust movements or shear versus flattening fabrics (Solar and Brown, 2001) are apparently less common.

An approximately 90° swing in stretching lineations across the different zones of the Kaoko Belt from strike-slip shear zones in the WKZ to over-thrusting onto the foreland margin reflects both a spatial and temporal progression in the reorientation of the tectonic transport direction during the Transpressional Phase. Deformation progressed from NNW–SSE-trending strike-slip movements to NW over SE oblique transpression in the Wrench-Stage to ultimately high-angle W over E transport and formation of large-scale over-folds and nappes in the latter Convergent-Stage (Fig. 16). This same progression is represented spatially from the orogen core to the foreland margin (Fig. 16). This temporal and spatial progression in deformation is also recognised in the Ugab Zone where second generation Transpressional Phase folds are dominant in the eastern margin (Figs. 10 and 17). Consequently, the horizontal and vertical stretch components of transpression (Dewey et al., 1998) are spread out over time through a continuous spectrum. Principal form surfaces that developed early in the Wrench-Stage were continually reworked during progressive deformation. Strain was continuously partitioned into the steep strike-slip shear zones in the orogen core (WKZ), even during Convergent-Stage nappe formation in the CKZ. These crustal-scale shear zones remained steep planar structures and were not folded by the nappe folds. Indeed Convergent-Stage over-folding and nappe development is fed by the continual reworking of the pervasive fabric in the shear zones. Consequently, the conventional temporal labelling of structures of distinct geometric style breaks down in the Kaoko Belt, because the regionally pervasive fabric was progressively reworked and continued to evolve throughout the formation of nappes and overfolds, that elsewhere (i.e. in the CKZ) fold the pervasive fabric.

Despite a temporal and spatial continuum in deformation and common structural history across the orogen, each tectonic zone is characterized by a distinct deformational style (Fig. 16). The core of the orogen, centred on the WKZ, is characterized by steep foliations, sinistral strike-slip movements and a very low-angle of oblique convergence and acts as a corridor of continuous deformation that feeds the margins of deformation in the CKZ and EKZ. The CKZ is characterized by large-scale refolding of the pervasive L–S fabric. Large-scale asymmetric folds and nappes with sub-horizontal axes all verge outwards onto the foreland in the east. This simple end-geometry formed through an evolving deformation regime from initiation in a wrench regime producing the L–S fabric, through progressively higher angles of convergence indicated by latest formed stretching lineations at higher angles to the orogen (Fig. 16).

The EKZ responded differently to Transpressional Phase orogenesis, is of much lower metamorphic grade and comprised of cratonic basement and platform carbonate sequence. It is therefore rheologically contrasted with the more mobile internal zones of the Kaoko Belt. Similar to Wrench-Stage fabrics in the rest of the Kaoko Belt, the EKZ also developed an early layer-parallel foliation with rare associated isoclines, but there is no strong linear component or evidence for intense non-coaxial shear. In contrast, deformation of the EKZ is dominated by later Convergent-Stage pure shear flattening at a high-angle to the length of the belt (Fig. 16). The deformation front of the belt progressed outwards from the earliest formed Wrench-Stage dominated core of the orogen to deformation being progressively later formed towards the margin and

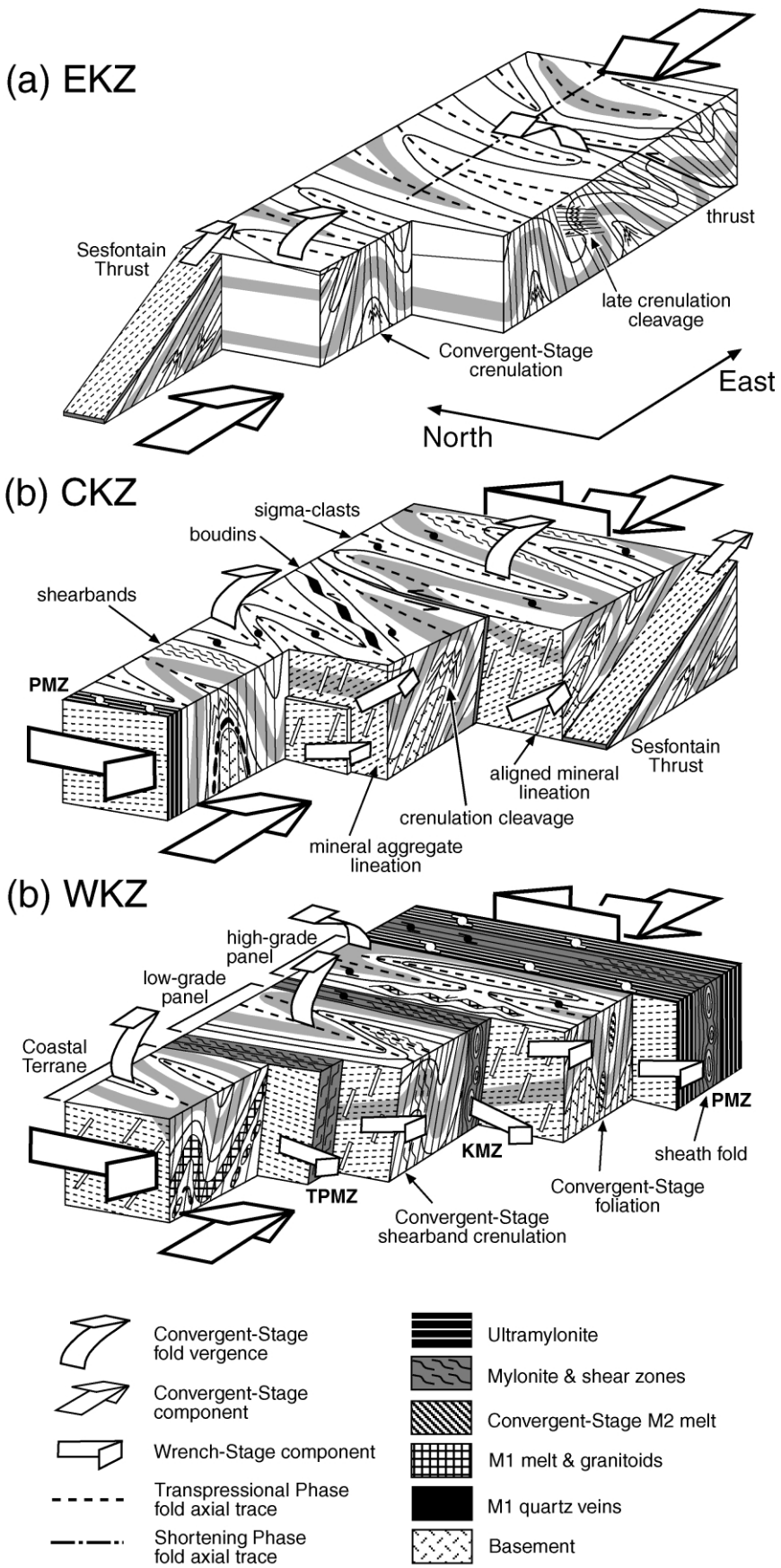

Fig. 16. Block diagrams illustrating the structural style and relationships between structural elements in each of the principal zones from east to west across the central Kaoko Belt. Arrows indicate components of transport during the Transpressional Phase. Shear zone abbreviations as in Fig. 2.

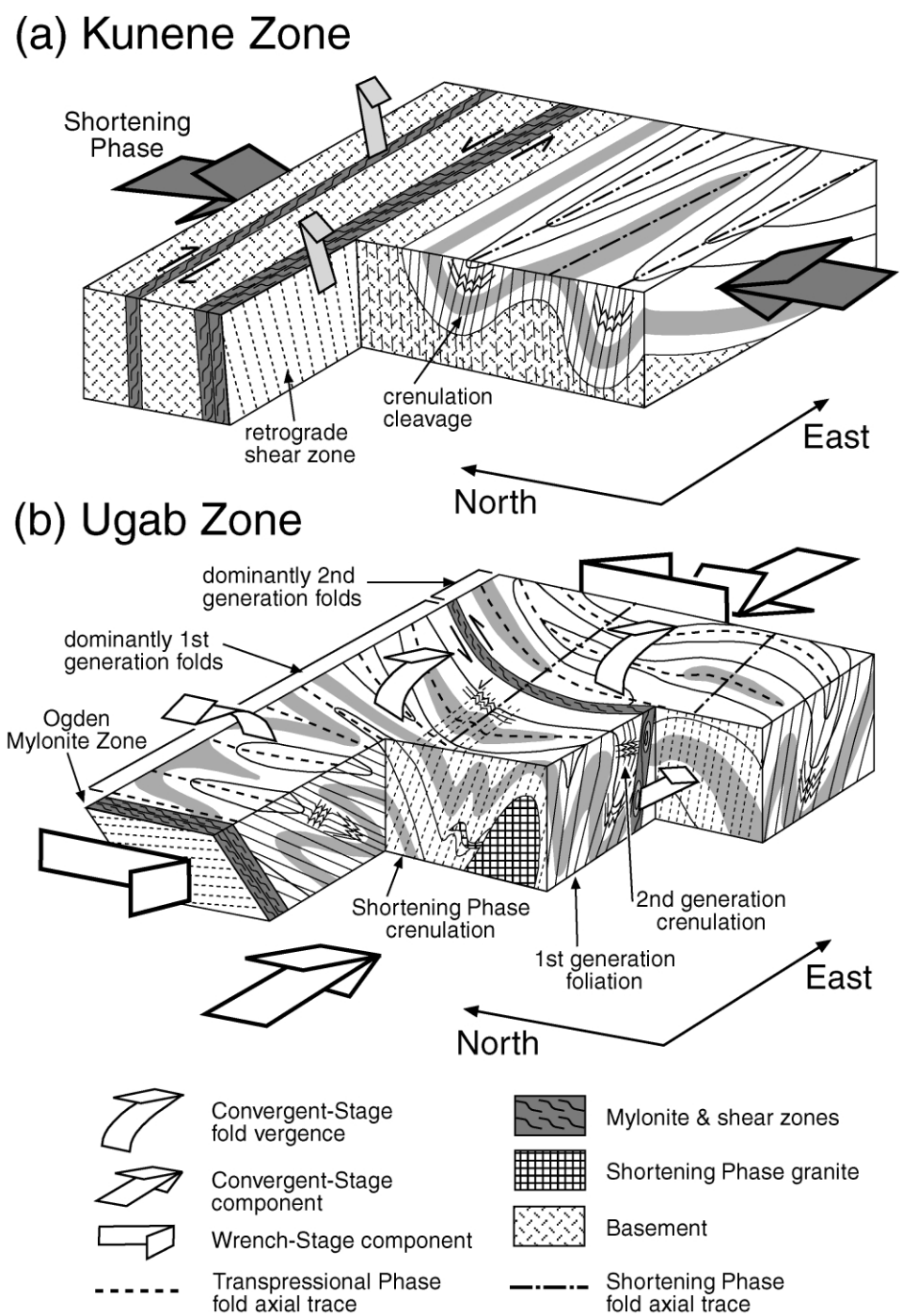

Fig. 17. Block diagrams illustrating the structural style and relationships between structural elements in the bounding marginal zones of the Kaoko Belt, the Kunene Zone in the northeast and the Ugab Zone in the south. Based on mapping and observations by the authors in both regions (Fig. 10). For clarity, arrows indicate components of main phase transport only in the respective regions: white—Transpressional Phase (dominant in the Ugab Zone); shaded—Shortening Phase (dominant in the Kunene Zone).

ultimately dominated by the later Convergent-Stage in the EKZ. Spatial progression of the deformation front and increasing dominance of successive stages in the temporal progression of deformation, across the belt (Figs. 16 and 17), implies that the width of the orogen increased outwards from the core as the Kaoko Belt evolved (cf. Robin and Cruden, 1994).

7.2. Regional implications

The Kaoko Belt illustrates three distinct deformation regimes in a rather protracted Pan-African Damara Orogeny: (1) an early Thermal Phase (M_1) apparently either without pervasive deformation or entirely obscured by subsequent deformations; (2) high-strain pervasive deformation and

metamorphic overprint (M_2) during the sinistral oblique Transpressional Phase; and (3) late-stage N–S shortening along the length of the belt. Analysis of the entire Kaoko Belt region recognises zones in which the three phases of the Damara Orogeny have been differentially partitioned. With extrapolation, these results give insights into the deformation history on a gross-scale for the entire Damara orogenic system. There has been speculation for a long time on how the geometry of the triple junction of the Damara Orogen operated during orogenesis. In particular, debate has centred on the relative timing of orogenesis/convergence of the three branches (Barnes and Sawyer, 1980; Coward, 1981, 1983; Porada et al., 1983; Hartnady et al., 1985, 1989; Dürr and Dingeldey, 1996). The outlined tectonothermal evolution of the Kaoko Belt can be correlated across the other crustal elements of the Damara Orogen, giving a coherent picture of crustal plate movements during the Pan-African Damara Orogeny. Evolution of the Kaoko Belt within the regional context precludes that all three arms of the Damara Orogen were deforming equally (in strain intensity and structural style) during any coeval deformational phase. Thus the triple junction geometry is the result of superimposed orogenic periods with distinct strain regimes and interacting plate geometries.

The Thermal Phase is recognised by early sheared granitoids with minumum ages of 656–630 and 580–552 Ma in the WKZ (Dingeldey, 1997; Seth et al., 1998) and 650–630 and 610–550 Ma in the Central Zone of the Inland Branch (i.e. Kröner, 1982; Miller, 1983). In the Kaoko Belt, deformation structures and mineral parageneses from the Thermal Phase were almost totally obliterated during subsequent intense deformation. In the Gariep Belt the Thermal Phase may be represented by the early subduction and closure phase at 576–573 Ma (Frimmel and Frank, 1998). Peak deformation, metamorphism and granite emplacement in the Dom Feliciano Belt in Brazil occurred in this period (Chemale et al., 1995; Da Silva et al., 1997). This early thermal and magmatic phase was apparently restricted to the core of the Damara Orogen, such as the western margins of the coastal arms and the Central Zone of the Inland Branch, and is absent from the Barrovian fold and thrust belt foreland margins. The tectonic environment of the Thermal Phase is poorly understood because early kinematic indicators and mineral parageneses are largely obliterated and beyond the scope of this paper.

Transpressional Phase SSE-directed oblique transport progressing to high-angle convergence onto the foreland, is recognised in both the Kaoko Belt and Gariep Belt (Gresse, 1994) coastal arms of the Damara Orogen. Sinistral transpression and the accompanying metamorphic overprint (M_2), occurred at much the same time in both coastal belts, approximately between 580 and 530 Ma (Frimmel, 1998; Frimmel and Frank, 1998; Seth et al., 1998). Progression from Wrench-Stage low-angle convergence to high-angle W over E transport in the Convergent-Stage is evident in the coastal arms. Identical deformation regime, transport vector and timing imply that the two coastal belts were contiguous and that the Congo and Kalahari Cratons were not widely separated at this time. This supports the view that closure of the inferred ocean basin along the site of the Inland Branch occurred early, at approximately 650 Ma as argued on stratigraphic grounds (Miller, 1983; Hoffman, 1994). The Central Zone of the Inland Branch also experienced orogenesis at the same time as the Transpressional Phase in the coastal arms. Granites of 570–540 Ma age (Kröner, 1982; Miller, 1983) are widespread in the Central Zone and early E–W-trending stretching lineations pre-date N–S convergence in the Shortening Phase (Coward, 1981; Oliver, 1994). Consequently, the entire western margin of the Damara Orogen experienced orogenesis during the Transpressional Phase, suggesting that the Congo and Kalahai Cratons acted as one contiguous continental plate with the outboard, obliquely colliding Rio De La Plata Craton in the west.

During the final Shortening Phase of the Damara Orogeny, the deformation front moved from the western margin, to within the African Plate, with N–S convergence between the Congo and Kalahai Cratons (Coward, 1983; Miller, 1983). Strain was very high within the Inland Branch (Coward, 1983; Miller, 1983; Oliver, 1994). Stretching lineations, tectonic transport directions and foreland-directed thrusting and over-folding at both margins of the Inland Branch are consistent with N–S to NNE–SSW convergence between the Congo and Kalahari Cratons (Coward, 1983; Miller, 1983). In contrast, the overprinting N–S shortening was minor in both coastal arms. However, moderate strains and upright folding was experienced at the terminations of the Kaoko Belt; the Kunene Zone in the northeast and Ugab Zone in the south (Figs. 12 and 17) and in the Northern Platform (Hedberg, 1979). N–S shortening of the Kaoko Belt occurred at some stage subsequent to shearing of WKZ granites with minimum ages between 580 and 552 Ma (Seth et al., 1998), and accompanied emplacement of the 530 Ma age syn-Shortening Phase granite in the Ugab Zone (Seth et al., 2000). Peak metamorphic parageneses, pervasive granite emplacement and the main phase of deformation in the Inland Branch occurred between 535 and 510 Ma (Miller, 1983; Oliver, 1994; Trompette, 1997; Jung et al., 2000). These age constraints and structural overprinting relationships in the Kaoko Belt (this paper) and elsewhere (Coward, 1981, 1983; Miller, 1983; Freyer and Halbich, 1994; Frimmel, 1998), constrain main phase N–S convergence in the Inland Branch to have occurred some 40–50 Ma after transpressional orogenesis in the coastal branches. The timing of N–S convergence between the Congo and Kalahari Cratons was remarkably consistent throughout the entire PAOS (Fig. 1), from the Inland Branch of the Damara Orogen, through the southern Lufilian Arc and Zambezi Belts into the Mozambique Belt in the west (Goscombe et al., 1998, 2000).

Appendix A
Summary of all geochronological data available from the Kaoko Belt and northern Namibia region

Terrane	Location	Stratigraphic unit	Rock-type	Method	Age (Ma)	Interpretation	Reference
Epupa Complex	Ruacana Falls	Epupa Metamorphic Complex	Granitic orthogneiss	U–Pb concordant (zircon)	1795 + 33/ − 29	Emplacement age	(1) Tegtmeyer and Kroner, 1985
Kamanjab Inlier	Franzfontein	Franzfontein Granite Suite	Granite	Rb–Sr (WR)	1547 ± 20	Emplacement age?	(2) Burger et al., 1976
Kamanjab Inlier	Franzfontein	Franzfontein Granite Suite	Granite	Rb–Sr (WR)	1580 ± 20	Deformation age	(2) Burger et al., 1976
Kamanjab Inlier	Franzfontein	Franzfontein Granite Suite	Granite	Rb–Sr (WR)	1800 ± 80	Emplacement age	(2) Burger et al., 1976
Kamanjab Inlier	North Namibia	Huab Complex	Granitic orthogneiss	U–Pb concordant (zircon)	1811 + 39/ − 35	Emplacement age	(1) Tegtmeyer and Kroner, 1985
Kamanjab Inlier	North Namibia	Huab Complex	Granitic orthogneiss	U–Pb concordant (zircon)	1749 + 78/ − 70	Emplacement age	(1) Tegtmeyer and Kroner, 1985
WKZ	Hoanib River	Pan-African granitoid	Orthogneiss	U–Pb SHRIMP (zircon)	565 ± 13	Emplacement age	(3) Seth et al., 1998
WKZ	Hoanib River	Pan-African granitoid	Orthogneiss	Pb–Pb evaporation (zircon)	563.8 ± 1.5	Emplacement age	(3) Seth et al., 1998
WKZ	Hoanib River	Pan-African granitoid	Orthogneiss	U–Pb SHRIMP (zircon)	656 ± 8	Emplacement age	(3) Seth et al., 1998
WKZ	Hoanib River	Pan-African granitoid	Orthogneiss	Pb–Pb evaporation (zircon)	567.2 ± 1.5	Emplacement minimum age	(3) Seth et al., 1998
WKZ	Hoanib River	Pan-African granitoid	Granitic orthogneiss	Pb–Pb evaporation (zircon)	551.9 ± 1.5	Emplacement minimum age	(3) Seth et al., 1998
WKZ	Hoanib River	Pan-African granitoid	Granitic orthogneiss	U–Pb SHRIMP (zircon)	580 ± 3	Emplacement age	(3) Seth et al., 1998
WKZ	Hoanib River	Pan-African granitoid	Granitic orthogneiss	U–Pb SHRIMP (zircon)	630 ± 8	Emplacement age	(3) Seth et al., 1998
WKZ	Skeleton Coast	Cretaceous dyke	Dolerite dyke	Ar–Ar versus K–Ar isochron	134.2 ± 0.9	Emplacement age	(4) Siendner and Mitchell, 1976
WKZ	Hoanib River	Mesoproterozoic Basement	Orthogneiss	U–Pb SHRIMP (zircon)	1507 ± 16	Upper concordia intercept age	(3) Seth et al., 1998
WKZ	Hoanib River	Mesooproterozoic Basement	Orthogneiss	Pb–Pb evaporation (zircon)	1335.4 ± 0.9	Emplacement age?	(3) Seth et al., 1998
WKZ	Hoanib River	Mesoproterozoic Basement	Orthogneiss	U–Pb SHRIMP (zircon)	578 ± 57	Lower concordia intercept age	(3) Seth et al., 1998
CKZ	Hoanib River	Andib Archaean Basement	Orthogneiss	U–Pb SHRIMP (zircon)	2605 ± 11	Emplacement age	(3) Seth et al., 1998
CKZ	Hoanib River	Andib Archaean Basement	Orthogneiss	U–Pb SHRIMP (zircon)	2287 ± 10	Emplacement age	(3) Seth et al., 1998
CKZ	Hoanib River	Andib Archaean Basement	Orthogneiss	U–Pb SHRIMP (zircon)	1985 ± 23	Emplacement age	(3) Seth et al., 1998
CKZ	Hoanib River	Andib Archaean Basement	Orthogneiss	U–Pb SHRIMP (zircon)	2645	Emplacement age	(3) Seth et al., 1998
CKZ	Hoanib River	Andib Archaean Basement	Orthogneiss	U–Pb SHRIMP (zircon)	1961 ± 4	Emplacement age	(3) Seth et al., 1998
CKZ	Hoanib River	Andib Archaean Basement	Orthogneiss	Pb–Pb evaporation (zircon)	2584.6 ± 0.4	Emplacement minimum age	(3) Seth et al., 1998
CKZ	Hoanib River	Andib Archaean Basement	Orthogneiss	Pb–Pb evaporation (zircon)	2584.2 ± 0.6	Emplacement minimum age	(3) Seth et al., 1998
CKZ	Hoanib River	Andib Archaean Basement	Orthogneiss	Pb–Pb evaporation (zircon)	2605.8 ± 0.6	Emplacement minimum age	(3) Seth et al., 1998
CKZ	Hoanib River	Andib Archaean Basement	Orthogneiss	U–Pb SHRIMP (zircon)	2616	Emplacement age	(3) Seth et al., 1998
CKZ	Hoanib River	Palaeoproterozoic Basement	Orthogneiss	U–Pb SHRIMP (zircon)	1972 ± 7	Emplacement age	(3) Seth et al., 1998
CKZ	Hoanib River	Palaeoproterozoic Basement	Orthogneiss	U–Pb SHRIMP (zircon)	1971 ± 7	Emplacement age	(3) Seth et al., 1998
CKZ	Sesfontein area	Khomas Subgroup	White mica schist	K–Ar (WR)	465 ± 12	Cooling or deformation age	(5) Ahrendt et al., 1983
CKZ	Sesfontein area	Nosib Group	White mica schist	K–Ar (WR)	494 ± 11	Cooling or deformation age	(5) Ahrendt et al., 1983
CKZ	Sesfontein area	Nosib Group	White mica schist	K–Ar (WR)	499 ± 11	Cooling or deformation age	(5) Ahrendt et al., 1983
EKZ	Sesfontein area	Mulden Group	White mica schist	K–Ar (WR)	479 ± 11	Cooling or deformation age	(5) Ahrendt et al., 1983
EKZ	Sesfontein area	Mulden Group	Mu–bi–chl schist	K–Ar (WR)	454 ± 11	Cooling or deformation age	(5) Ahrendt et al., 1983
EKZ	Sesfontein area	Mulden Group	Mu–bi–chl schist	K–Ar (WR)	442 ± 11	Cooling or deformation age	(5) Ahrendt et al., 1983
EKZ	Sesfontein area	Mulden Group	Mu–bi–chl schist	K–Ar (WR)	463 ± 11	Cooling or deformation age	(5) Ahrendt et al., 1983
EKZ	Sesfontein area	Mulden Group	Mu–bi–chl schist	K–Ar (WR)	459 ± 12	Cooling or deformation age	(5) Ahrendt et al., 1983
EKZ	Sesfontein area	Mulden Group	White mica shist	K–Ar (WR)	487 ± 11	Cooling or deformation age	(5) Ahrendt et al., 1983
EKZ	Sesfontein area	Mulden Group	Mu–bi–chl schist	K–Ar (WR)	469 ± 11	Cooling or deformation age	(5) Ahrendt et al., 1983
EKZ	Sesfontein area	Mulden Group	Mu–bi–chl schist	K–Ar (WR)	460 ± 11	Cooling or deformation age	(5) Ahrendt et al., 1983
EKZ	Sesfontein area	Tsumeb Subgroup	Mu–bi–chl schist	K–Ar (WR)	460 ± 11	Cooling or deformation age	(5) Ahrendt et al., 1983
Ugab Zone	Huab River mouth	Pan-African granitoid	Granite	U–Pb concordant (zircon)	570 ± 20	Emplacement age	(6) Miller and Burger, 1983
Ugab Zone	Voetspoor Intrusion	Pan-African granitoid	Syenite	Pb–Pb evapouration (zircon)	530 ± 3	Emplacement age	(13) Seth et al., 2000
Ugab Zone	Toscanini borehole	Mulden Group	Mu–bi–chl schist	K–Ar (WR)	380 ± 10	Cooling or deformation age	(5) Ahrendt et al., 1983
Ugab Zone	Toscanini borehole	Mulden Group	Mu–bi–chl schist	K–Ar (WR)	427 ± 10	Cooling or deformation age	(5) Ahrendt et al., 1983
Ugab Zone	Toscanini borehole	Mulden Group	Mu–bi–chl schist	K–Ar (WR)	428 ± 10	Cooling or deformation age	(5) Ahrendt et al., 1983

Appendix A (*continued*)

Terrane	Location	Stratigraphic unit	Rock-type	Method	Age (Ma)	Interpretation	Reference
Ugab Zone	Brandberg West	Khomas Subgroup	Mu–bi–chl schist	K–Ar (WR)	422 ± 10	Cooling or deformation age	(5) Ahrendt et al., 1983
Ugab Zone	Brandberg West	Khomas Subgroup	Mu–bi–chl schist	K–Ar (WR)	418 ± 10	Cooling or deformation age	(5) Ahrendt et al., 1983
Ugab Zone	Brandberg West	Khomas Subgroup	Mu–bi–chl schist	K–Ar (WR)	431 ± 10	Cooling or deformation age	(5) Ahrendt et al., 1983
Ugab Zone	Brandberg West	Khomas Subgroup	White mica schist	K–Ar (WR)	490 ± 11	Cooling or deformation age	(5) Ahrendt et al., 1983
Ugab Zone	Doros area	Late-tect, Salem type	Late-tectonic syenite	Rb–Sr (WR)	573 ± 33	Emplacement age	(7) Kröner, 1982
Ugab Zone	Ugab River (10m)	Damara Sequence	Meta-sediment	Fission track (apatite)	109.8 ± 3.5	Cooling age	(8) Brown et al., 1990
Ugab Zone	Ugab River (0m)	Damara Sequence	Meta-sediment	Fission track (apatite)	106.8 ± 3.9	Cooling age	(8) Brown et al., 1990
Ugab Zone	Ugab River (440m)	Damara Sequence	Meta-sediment	Fission track (apatite)	91.0 ± 2.5	Cooling age	(8) Brown et al., 1990
Ugab Zone	Ugab River (660m)	Damara Sequence	Meta-sediment	Fission track (apatite)	100.8 ± 5.3	Cooling age	(8) Brown et al., 1990
Ugab Zone	Ugab River (790m)	Damara Sequence	Meta-sediment	Fission track (apatite)	81.4 ± 3.5	Cooling age	(8) Brown et al., 1990
Ugab Zone	Ugab River (690m)	Damara Sequence	Meta-sediment	Fission track (apatite)	81.0 ± 2.9	Cooling age	(8) Brown et al., 1990
Ugab Zone	Ugab River (1570m)	Damara Sequence	Meta-sediment	Fission track (apatite)	90.7 ± 3.8	Cooling age	(8) Brown et al., 1990
Ugab Zone	Cape Cross	Cretaceous dyke	Dolerite dyke	K–Ar (WR)	124 ± 6	Emplacement	(4) Siendner and Mitchell, 1976
Ugab Zone	Cape Cross	Cretaceous dyke	Dolerite dyke	K–Ar (WR)	139 ± 7	Emplacement	(4) Siendner and Mitchell, 1976
Ugab Zone	Messum	Cretaceous dyke	Dolerite dyke	K–Ar (WR)	142 ± 4	Emplacement	(4) Siendner and Mitchell, 1976
North Platform	Tsumeb Mine	Pan-African mineralization	Pb–Zn–Cu sulphide	Pb–Pb model (galena)	530 ± 11	Syn-tectonic mineralization	(9) Kamona et al., 1999
North Platform	Etosha strat test 1	U Mulden G, Owambo F	Shale	K–Ar (WR)	455 ± 13	Tectonothermal event	(10) Clauer and Kroner, 1979
North Platform	Etosha strat test 1	U Mulden G, Owambo F	Shale	K–Ar (WR)	535 ± 13	Tectonothermal event	(10) Clauer and Kroner, 1979
North Platform	Etosha strat test 1	U Mulden G, Owambo F	Shale	K–Ar (WR)	550–560 ± 14	Deposition age	(10) Clauer and Kroner, 1979
Northern Zone	Oas Farm	Upper Nosib Group	Quartz syenite	U–Pb concordant (zircon)	756 ± 2	Deposition minimum age	(11) Hoffman et al., 1996
Northern Zone	Summas Mountains	Upper Nosib Group	Ash-flow tuff	U–Pb concordant (zircon)	746 ± 2	Eruption age	(11) Hoffman et al., 1996
Northern Zone	Summas Mountains	Lower Ugab Group	Rhyolite lava flow	U–Pb concordant (zircon)	747 ± 2	Eruption age	(11) Hoffman et al., 1996
Etendeka Plateau	Etendeka Plateau	Etendeka Group	Basalt flow	K–Ar (WR)	114–117 ± 2	Eruption age	(12) Gidskehaug et al., 1975
Etendeka Plateau	Etendeka Plateau	Etendeka Group	Basalt flow	K–Ar (WR)	122–125 ± 2	Eruption age	(12) Gidskehaug et al., 1975
Etendeka Plateau	Etendeka Plateau	Etendeka Group	Basalt flow	K–Ar (WR)	107–110 ± 2	Eruption age	(12) Gidskehaug et al., 1975
Etendeka Plateau	Etendeka Plateau	Etendeka Group	Basalt flow	K–Ar (WR)	119–128 ± 2	Eruption age	(12) Gidskehaug et al., 1975
Etendeka Plateau	Etendeka Plateau	Etendeka Group	Dolerite sill	K–Ar (WR)	93–94 ± 2	Emplacement age	(12) Gidskehaug et al., 1975
Etendeka Plateau	Etendeka Plateau	Etendeka Group	Basalt flow	K–Ar (WR)	114 ± 6	Eruption age	(4) Siendner and Mitchell, 1976
Etendeka Plateau	Etendeka Plateau	Etendeka Group	Basalt flow	K–Ar (WR)	112 ± 3	Eruption age	(4) Siendner and Mitchell, 1976
Etendeka Plateau	Etendeka Plateau	Etendeka Group	Basalt flow	K–Ar (WR)	110 ± 3	Eruption age	(4) Siendner and Mitchell, 1976
Etendeka Plateau	Etendeka Plateau	Etendeka Group	Basalt flow	K–Ar (WR)	114 ± 3	Eruption age	(4) Siendner and Mitchell, 1976
Etendeka Plateau	Etendeka Plateau	Etendeka Group	Basalt flow	K–Ar (WR)	117 ± 3	Eruption age	(4) Siendner and Mitchell, 1976
Etendeka Plateau	Cape Cross	Etendeka Group	Basalt flow	K–Ar (WR)	110 ± 3	Eruption age	(4) Siendner and Mitchell, 1976
Etendeka Plateau	Cape Cross	Etendeka Group	Basalt flow	K–Ar (WR)	117 ± 3	Eruption age	(4) Siendner and Mitchell, 1976
Etendeka Plateau	Etendeka Plateau	Etendeka Group	Basalt flows	Ar–Ar versus K–Ar isochron	121 ± 1.2	Eruption age	(4) Siendner and Mitchell, 1976

Number of reference is referred to in Table 1.

Appendix B

Estimates of dominant fabric strain ratio ($R = X/Z$) and shear strain (γ). Strain estimates are discussed in text and summarised in Figs. 5 and 6

Location	Rock type	Deformed clasts, quartz fringes and boudins							S–C′ fabric		Sheath folds			
		X	Y	Z	R	k	γa	n	θ	γb	α	B/C	γc	n
Aspect ratio of deformed clasts in diamictite and conglomerate (averages)														
K1066	QFG clast shistosic gneiss	7.05	1.00	0.22	32.05	1.55	5.48	8						
K1110	Quartzite clast diamictite	5.67	1.00	0.27	21.00	1.53	4.36	13						
K19	QFG clast conglomerate	10.00	1.00	0.30	33.33	3.00	5.60	1						
K198	QFG clast diamictite	2.52	1.00	0.31	8.13	0.78	2.48	13						
K361	QFG clast conglomerate	1.93	1.00	0.23	8.39	0.44	2.53	19						
K465	Carbonate clast diamictite	7.32	1.00	0.49	14.94	3.59	3.60	7						
K57	QFG clast conglomerate	3.17	1.00	0.27	11.74	0.86	3.12	9						
K66	QFG clast conglomerate	3.09	1.00	0.27	11.44	0.83	3.07	16						
K821	Quartzite clast conglomerate	3.50	1.00	0.23	15.22	0.81	3.64	9						
Aspect ratio of quartz fibre fringes on magnetite (average, plane strain assumed)														
KK143	Quartz–sericite schist	3.75	1.00	0.28	14.46	1.00	3.46	10						
Degree of stretch of layer-parallel boudin trains (plane strain assumed)														
K1013	Drawn boudins	1.35	1.00	0.74	1.82	1.00	–	1						
K1014	Drawn boudins	1.16	1.00	0.86	1.35	1.00	–	1						
K1036	Drawn boudins	3.50	1.00	0.29	12.25	1.00	3.20	1						
K1040	Drawn boudins	1.27	1.00	0.79	1.61	1.00	–	1						
K1053	Drawn boudins	2.06	1.00	0.49	4.24	1.00	1.50	1						
K1134	Drawn boudins	2.35	1.00	0.43	5.52	1.00	1.88	1						
K1135	Drawn boudins	2.39	1.00	0.42	5.71	1.00	1.93	1						
K1150	Drawn boudins	1.69	1.00	0.59	2.87	1.00	0.93	1						
K1152	Drawn boudins	1.83	1.00	0.55	3.36	1.00	1.17	1						
K1186	Drawn boudins	1.17	1.00	0.86	1.36	1.00	–	1						
K1188	Drawn boudins	1.67	1.00	0.60	2.78	1.00	0.88	1						
K1200	Drawn boudins	1.79	1.00	0.56	3.20	1.00	1.10	1						
K1216	Drawn boudins	1.50	1.00	0.67	2.25	1.00	0.50	1						
K1253	Drawn boudins	2.25	1.00	0.44	5.05	1.00	1.75	1						
K1255	Drawn boudins	1.53	1.00	0.65	2.34	1.00	0.59	1						
K1256	Drawn boudins	3.16	1.00	0.32	9.99	1.00	2.83	1						
K1268	Drawn boudins	2.60	1.00	0.38	6.76	1.00	2.18	1						
K1339	Drawn boudins	4.04	1.00	0.25	16.32	1.00	3.78	1						
K41	Drawn boudins	1.75	1.00	0.57	3.06	1.00	1.03	1						
K45	Drawn boudins	6.00	1.00	0.17	36.00	1.00	5.83	1						
K737	Drawn boudins	1.45	1.00	0.69	2.10	1.00	0.32	1						
K797	Drawn boudins	2.33	1.00	0.43	5.43	1.00	1.85	1						
K858	Drawn boudins	1.38	1.00	0.72	1.90	1.00	–	1						
K955	Drawn boudins	1.10	1.00	0.91	1.21	1.00	–	1						
K985	Drawn boudins	1.37	1.00	0.73	1.88	1.00	–	1						
K990	Drawn boudins	1.54	1.00	0.65	2.37	1.00	0.61	1						
K?	Drawn boudins	2.00	1.00	0.50	4.00	1.00	1.41	1						
K1003	Shearband boudins	1.61	1.00	0.62	2.59	1.00	0.77	1						
K1008	Shearband boudins	1.54	1.00	0.65	2.39	1.00	0.62	1						
K1036	Shearband boudins	1.35	1.00	0.74	1.84	1.00	–	1						
K1040	Shearband boudins	1.13	1.00	0.89	1.27	1.00	–	1						
K1103	Shearband boudins	1.33	1.00	0.75	1.78	1.00	–	1						
K1133	Shearband boudins	1.17	1.00	0.86	1.36	1.00	–	1						
K1134	Shearband boudins	1.25	1.00	0.80	1.57	1.00	–	1						
K1135	Shearband boudins	1.49	1.00	0.67	2.22	1.00	0.47	1						
K1136	Shearband boudins	2.03	1.00	0.49	4.14	1.00	1.46	1						
K1151	Shearband boudins	2.17	1.00	0.46	4.70	1.00	1.64	1						
K1165	Shearband boudins	1.45	1.00	0.69	2.11	1.00	0.33	1						
K1186	Shearband boudins	1.71	1.00	0.58	2.94	1.00	0.97	1						
K1200	Shearband boudins	1.72	1.00	0.58	2.96	1.00	0.98	1						
K1201	Shearband boudins	1.98	1.00	0.51	3.91	1.00	1.38	1						
K1208	Shearband boudins	2.23	1.00	0.45	4.97	1.00	1.72	1						
K1216	Shearband boudins	1.26	1.00	0.79	1.59	1.00	–	1						
K1254	Shearband boudins	1.41	1.00	0.71	1.99	1.00	–	1						
K1255	Shearband boudins	2.43	1.00	0.41	5.89	1.00	1.97	1						

Appendix B (*continued*)

Location	Rock type	Deformed clasts, quartz fringes and boudins							S–C′ fabric		Sheath folds			
		X	*Y*	*Z*	*R*	*k*	γa	*n*	*θ*	γb	*α*	*B/C*	γc	*n*
K1256	Shearband boudins	2.63	1.00	0.38	6.92	1.00	2.22	1						
K1259	Shearband boudins	1.24	1.00	0.81	1.54	1.00	–	1						
K1266	Shearband boudins	2.31	1.00	0.43	5.33	1.00	1.83	1						
K1268	Shearband boudins	1.53	1.00	0.65	2.35	1.00	1.53	1						
K1271	Shearband boudins	1.14	1.00	0.88	1.30	1.00	–	1						
K1276	Shearband boudins	1.26	1.00	0.80	1.58	1.00	–	1						
K1311	Shearband boudins	1.18	1.00	0.85	1.38	1.00	–	1						
K1335	Shearband boudins	1.46	1.00	0.69	2.13	1.00	0.36	1						
K1337	Shearband boudins	4.88	1.00	0.20	23.84	1.00	4.67	1						
K41	Shearband boudins	2.24	1.00	0.45	5.02	1.00	1.74	1						
K493	Shearband boudins	2.95	1.00	0.34	8.70	1.00	2.59	1						
K54	Shearband boudins	1.23	1.00	0.81	1.52	1.00	≠	1						
K59	Shearband boudins	1.33	1.00	0.75	1.77	1.00	–	1						
K663	Shearband boudins	1.62	1.00	0.62	2.62	1.00	0.79	1						
K725	Shearband boudins	1.93	1.00	0.52	3.72	1.00	1.31	1						
K737	Shearband boudins	2.09	1.00	0.48	4.38	1.00	1.54	1						
K820	Shearband boudins	1.88	1.00	0.53	3.55	1.00	1.24	1						
K821	Shearband boudins	1.42	1.00	0.71	2.01	1.00	0.07	1						
K984	Shearband boudins	1.76	1.00	0.57	3.09	1.00	1.04	1						
K987	Shearband boudins	2.20	1.00	0.45	4.85	1.00	1.69	1						
K988	Shearband boudins	1.27	1.00	0.79	1.61	1.00	–	1						
KK102	Shearband boudins	3.07	1.00	0.33	9.41	1.00	2.72	1						
KK104	Shearband boudins	1.54	1.00	0.65	2.36	1.00	0.60	1						
KK114	Shearband boudins	2.39	1.00	0.42	5.69	1.00	1.92	1						
KK114	Shearband boudins	4.60	1.00	0.22	21.13	1.00	4.37	1						
KK44	Shearband boudins	1.33	1.00	0.75	1.76	1.00	–	1						
KK51	Shearband boudins	1.39	1.00	0.72	1.92	1.00	–	1						
KK51	Shearband boudins	1.72	1.00	0.58	2.96	1.00	0.98	1						
KK86	Shearband boudins	1.53	1.00	0.66	2.33	1.00	0.57	1						
Angular relationship between shearbands and pervasive foliation (assuming simple shear)														
K	Greywacke schist								35.0	0.73				
K	Greywacke schist								27.0	1.45				
K1014	Greywacke schist								27.0	1.45				
K239	Schistosic gneiss								20.0	2.38				
K353	Schistosic gneiss								29.0	1.25				
K369	Greywacke schist								30.0	1.15				
K376	Schistosic gneiss								12.0	4.49				
K455	Augen gneiss								26.0	1.56				
K494	Greywacke schist								29.0	1.25				
K500	Greywacke schist								24.5	1.74				
K502	Greywacke schist								21.0	2.22				
K620	Greywacke schist								23.0	1.93				
K92	Greywacke schist								19.0	2.56				
KK102	Greywacke schist								28.0	1.35				
KK104	Greywacke schist								22.0	2.07				
KK107	Greywacke schist								35.0	0.73				
KK112	Greywacke schist								16.0	3.20				
KK112	Greywacke schist								16.0	3.20				
KK125	Greywacke schist								20.0	2.38				
KK125	Greywacke schist								20.0	2.38				
KK127	Greywacke schist								27.0	1.45				
KK127	Greywacke schist								16.0	3.20				
KK128	Greywacke schist								16.0	3.20				
KK129	Greywacke schist								23.0	1.93				
KK139	Greywacke schist								18.0	2.75				
KK140	Greywacke schist								11.0	4.95				
KK2	Greywacke schist								35.0	0.73				
KK63	Greywacke schist								18.0	2.75				
KK64	Greywacke schist								10.0	5.49				
KK65	Greywacke schist								35.0	0.73				

(*continued on next page*)

Appendix B (*continued*)

Location	Rock type	Deformed clasts, quartz fringes and boudins							S–C′ fabric		Sheath folds			
		X	*Y*	*Z*	*R*	*k*	γa	*n*	θ	γb	α	*B*/*C*	γc	*n*
KK66	Greywacke schist								20.0	2.38				
KK80	Greywacke schist								16.0	3.20				
KK80	Greywacke schist								17.0	2.97				
KK81	Felsic mylonite								20.0	2.38				
KK87	Greywacke schist								22.0	2.07				
KK87	Greywacke schist								27.0	1.45				
KK87	Greywacke schist								24.0	1.80				
KK87	Greywacke schist								24.0	1.80				
KK89	Greywacke schist								25.0	1.68				
Ogden rocks	Greywacke schist								28.0	1.35				
Sheath fold geometry (assuming simple shear)														
K322	Greywacke schist										11.0	2.4	12.31	1
K324	Greywacke schist										10.5	2.9	15.62	1
K341	Greywacke schist										12.0	2.2	10.3	1
K871	Greywacke schist										9.5	2.9	17.3	1
K968	Greywacke schist										10.0	3.0	16.98	1
KK114	Greywacke schist										20.0	3.0	8.18	1
KK1156	Greywacke schist										9.0	3.6	22.71	1
KK119	Greywacke schist										9.0	3.0	18.91	1
KK119	Greywacke schist										38.0	3.0	3.71	1
KK119	Greywacke schist										25.0	3.0	6.36	1
KK1231	Greywacke schist										10.0	3.6	20.39	1
KK27	Greywacke schist										20.0	3.0	8.18	1
KK27	Greywacke schist										20.0	3.0	8.18	1
KK99	Greywacke schist										11.2	3.1	19.80	5
KK99	Greywacke schist										17.4	3.0	10.10	7

Shear strain (γc) is calculated from the aspect ratio of sheath folds (*B*/*C*) and angle between margin of sheaths and stretching lineation (θ), assuming simple shear and the function: $\alpha = \arctan[(B/C).1/(\sqrt{(\gamma 2 + 1)})]$ (Lacassin and Mattauer, 1985). Shear strain (γa) is calculated assuming simple shear and the simplified function: $X/Z = \gamma^2 + 2$ (Ramsay, 1967). $k = (X/Y)/(Y/Z)$ (Ramsay, 1967). Shear strain (γb) is calculated from the acute angle between S- and C′-planes (θ), assuming simple shear and the function: $\gamma = 2/(\tan(2\theta))$ (Ramsay and Graham, 1970).

Acknowledgements

Murray Hasseler and Bonza are sincerely thanked for their great company in the field. Cees Passchier, Rudolph Trouw, Roy Miller and Charlie Hoffman are thanked for the discussions we had while 'reading the rocks'. This research resulted from fieldwork undertaken for the Namibian Geological Survey (1997–1999), Anglo-American (1999), privately funded work (1997–2000), Namibian Geological Survey car support awarded to Prof. Cees Passchier (1999) and ARC Discovery Grant awarded to Prof. David Gray (2001). Adelaide University, Monash University and Pearce Hardware are sincerely thanked for their support during the writing up of this work. The work in Namibia benefited greatly from the administrative support of the legendary Mimi Duneski. Bob Holdsworth, Grahame Oliver and Tom Blenkinsop are thanked for their helpful and innovative suggestions for the manuscript.

References

Ahrendt, H., Behr, H.-J., Clauer, N., Hunzinker, J.C., Porada, H., Weber, K., 1983. The Northern Branch: Depositional Development and Timing of the Structural and Metamorphic Evolution within the Framework of the Damara Orogen, Springer-Verlag, Berlin, pp. 723–743.

Bale, P., Brun, J.-P., 1989. Late Precambrian thrust and wrench zones in northern Brittany (France). Journal of Structural Geology 11, 391–405.

Barnes, S.-J., Sawyer, E.W., 1980. An alternative model for the Damara Mobile Belt: ocean crust subduction and continental convergence. Precambrian Research 13, 297–336.

Berthe, D., Brun, J.P., 1980. Evolution of folds during progressive shear in the South Armorican Shear Zone, France. Journal of Structural Geology 2, 127–133.

Berthe, D., Choukroune, P., Jegouzo, P., 1979. Orthogneiss, mylonite and noncoaxial deformation of granites: the example of the South Armorican Shear Zone. Journal of Structural Geology 1, 31–42.

Brown, R.W., Gleadow, A.J.W., Summerfield, M.A., Rust, D., 1990. The morphotectonic development of the continental margin of south western Africa: new evidence from fission track analysis. De Beers Report August 1988.

Burg, J.P., Laurent, Ph., 1978. Strain analysis of a shear zone in a granodiorite. Tectonophysics 47, 15–42.

Burger, A.J., Clifford, T.N., Miller, R.Mc.G., 1976. Zircon U–Pb ages of the Franzfontein Granitic Suite. Northern South West Africa. Precambrian Research 3, 415–431.

Chemale, F., Walraven, F., Hartmann, L.A., da Silva, L.C., Gresse, P.G., 1994. Pb/Pb zircon dating of the Dom Feliciano Belt, southern Brazil. In: Niall, M., McManus, C. (Eds.), Proterozoic Crustal and Metallogenic Evolution. Abstracts of Geological Society and Geological Survey of Namibia 8, Windhoek.

Chemale, J.F., Hartmann, L.A., da Silva, L.C., 1995. Stratigraphy and tectonics of Precambrian to early Palaeozoic units in Southern Brazil and Uruguay. Acta Geologica Leopoldensia 44, 1–111.

Clauer, N., Kröner, A., 1979. Strontium and argon isotopic homogenization of pelitic sediments during low-grade regional metamorphism: the Pan-African Upper Damara Sequence of northern Namibia. Earth Planetary Science Letters 43, 117–131.

Cobbold, P.R., Quinquis, H., 1980. Development of sheath folds in shear regimes. Journal of Structural Geology 2, 119–126.

Comacho, A., McDougall, I., 2000. Intracratonic, strike-slip partitioned transpression and the formation and exhumation of eclogite facies rocks: an example from the Musgrave Block, central Australia. Tectonics 19, 978–996.

Coward, M.P., 1981. The junction between Pan African Mobile belts in Namibia: its structural history. Tectonophysics 76, 59–73.

Coward, M.P., 1983. The tectonic history of the Damara belt. In: Miller, R.McG. (Ed.), Evolution of the Damara Orogen; Special Publication of the Geological Society of South Africa 11, pp. 409–421.

Da Silva, L.C., McNaughton, N.J., Hartmann, L.A., Fletcher, I.R., Gresse, P., Scheepers, R., 1997. U–Pb (SHRIMP) isotopic constraints for the evolution of southern Brazilian granitic province, and some correlated South African, Pan-African plutons. Second International Symposium on Granites and Associated Mineralization, Salvador, pp. 276–277.

Davies, C.J., Coward, M.P., 1982. The structural evolution of the Gariep Arc in southern Namibia (South-West Africa). Precambrian Research 17, 173–198.

Dewey, J.F., Holdsworth, R.E., Strachan, R.A., 1998. Transpression and transtension zones. In: Holdsworth, R.E., Strachan, R.A., Dewey, J.F. (Eds.), Continental Transpressional and Transtensional Tectonics. Geological Society, London, Special Publications 135, pp. 1–14.

Dingeldey, D.P., 1997. Tectono-Metamorphic Evolution of the Pan-African Kaoko Belt, NW-Namibia. Ph.D. Thesis. Julius-Maximilians-Universitat, Wurzburg, 246pp.

Dingeldey, D.P., Dürr, S.B., Charlesworth, E.G., Franz, L., Okrusch, M., Stanistreet, I.G., 1994. A geotraverse through the northern coastal branch of the Damaran Orogen west of Sesfontein, Namibia. Journal of African Earth Science 19, 315–329.

Dürr, S.B., Dingeldey, D.P., 1996. The Kaoko belt (Namibia): part of a late Neoproterozoic continental-scale strike-slip system. Geology 24, 503–506.

Ebert, H.D., Hasui, Y., 1998. Transpressional tectonics and strain partitioning during oblique collision between three plates in the Precambrian of southeast Brazil. In: Holdsworth, R.E., Strachan, R.A., Dewey, J.F. (Eds.), Continental Transpressional and Transtensional Tectonics. Geological Society, London, Special Publications 135, pp. 231–252.

Ellis, M.A., 1986. Structural morphology and associated strain in the central Cordillera (British Columbia and Washington): evidence of oblique tectonics. Geology 14, 647–650.

Folling, P.G., Frimmel, H.E., Zartman, R.E., 1998. Chemostratigraphical correlation and Pb–Pb dating of metasedimentary sequences in the Gariep Belt: evidence for two different diamictites. In: Almond, J., Anderson, J., Booth, P., Chinsamy-Turan, A., Cole, D., de Wit, M.J., Rubridge, B., Smith, R., Storey, B.C., van Bever Donker, J. (Eds.), Gondwana 10: Event Stratigraphy of Gondwana. Journal of African Earth Sciences 27/1A, pp. 76–77.

Freyer, E.E., Halbich, I.W., 1994. Deformation history of the lower Ugab Belt. In: Niall, M., McManus, C. (Eds.), Proterozoic Crustal and Metallogenic Evolution. Abstracts of Geological Society and Geological Survey of Namibia Conference 18, Windhoek.

Frimmel, H.E., 1995. Metamorphic evolution of the Gariep Belt. South African Tydskr. Geology 98, 176–190.

Frimmel, H.E., 1996. New Pb–Pb single zircon age constraints on the timing of neoproterozoic glaciation and continental break-up in Namibia. The Journal of Geology 104, 459–469.

Frimmel, H.E., 1998. Neoproterozoic/Early Cambrian amalgamation of southern South America and Africa: the Gariepian perspective. In: Almond, J., Anderson, J., Booth, P., Chinsamy-Turan, A., Cole, D., de Wit, M.J., Rubridge, B., Smith, R., Storey, B.C., van Bever Donker, J. (Eds.), Gondwana 10: Event Stratigraphy of Gondwana. Journal of African Earth Sciences 27/1A, pp. 78–79.

Frimmel, H.E., Frank, W., 1998. Neoproterozoic tectono-thermal evolution of the Gariep Belt and its basement, Namibia and South Africa. Precambrian Research 90, 1–28.

Goscombe, B.D., 1998. Preliminary report on the geology of the Opuwo sheet, Kaoko Belt, Namibia. Geological Survey of Namibia Report.

Goscombe, B.D., 1999. Geological report on magnetic and radiometric anomalies mapped in the region south of the Kunene Igneous Complex, Namibia. Company exploration reports, Geological Survey of Namibia.

Goscombe, B.D., 1999. Geological map of the Sesfontein 1:250,000 sheet. Geological Survey of Namibia.

Goscombe, B.D., 1999. Geological map of Tomakas 1:50,000 sheet. Geological Survey of Namibia.

Goscombe, B.D., 1999. Geological map of Omapungwe 1:50,000 sheet. Geological Survey of Namibia.

Goscombe, B.D., 1999. Geological map of Orumpembe 1:50,000 sheet. Geological Survey of Namibia.

Goscombe, B., Hand, M., 2001. Tectonometamorphic Evolution of the Kaoko Belt, Namibia. Geological Society of Australia abstracts, Specialist Group in Tectonics and Structural Geology, Conference, Ulverstone, Abstracts 64, 61.

Goscombe, B.D., Passchier, C., 2002. Asymmetric boudins as shear sense indicators — an assessment from field data. Journal of Structural Geology 25, 575–589.

Goscombe, B.D., Trouw, R., 1998. The geometry of folded tectonic shear sense indicators. Journal of Structural Geology 21, 123–127.

Goscombe, B.D., Armstrong, R., Barton, J.M., 1998. Tectonometamorphic evolution of the Chewore Inliers: partial re-equilibration of high-grade basement during the Pan-African Orogeny. Journal of Petrology 39, 1347–1384.

Goscombe, B.D., Armstrong, R., Barton, J.M., 2000. Geology of the Chewore Inliers: constraining the Mesoproterozoic to Palaeozoic evolution of the Zambezi Belt. Journal of African Earth Science 30, 589–627.

Goscombe, B.D., Hand, M., Gray, D., Mawby, J., 2002. Contemporaneous granulite and Barrovian metamorphism in a transpressional orogen: the Kaoko Belt, Namibia. Journal of Petrology (submitted).

Gresse, P.G., 1994. Strain partitioning in the southern Gariep Arc as reflected by sheath folds and stretching directions. South Africa Journal of Geology 97, 52–61.

Guj, P., 1970. The Damara Mobile Belt in the south-western Kaokoveld, South-West Africa. Ph.D. Thesis, University of Cape Town, 168pp.

Hälbich, I.W., Alchin, D.J., 1995. The Gariep belt: stratigraphic-structural evidence for obliquely transformed grabens and back-folded thrust stacks in a combined thick-skin thin-skin structural setting. Journal of African Earth Sciences 21 (1), 9–33.

Hansen, V.L., 1989. Structural and kinematic evolution of the Teslin suture zone, Yukon: record of an ancient transpressional margin. Journal of Structural Geology 11, 717–733.

Haq, S.S.B., Davis, D.M., 1997. Oblique convergence and the lobate mountain belts of western Pakistan. Geology 25, 23–26.

Harland, W.B., 1971. Tectonic transpression in Caledonian Spitsbergen. Geologocal Magazine 108, 27–42.

Hartnady, C.J.H., Joubert, P., Stowe, C., 1985. Proterozoic crustal evolution in Southwestern Africa. Episodes 8, 236–244.

Hartnady, C.J.H., Hoffmann, K.H., Von Veh, M.W., 1989. Tectonic evolution of the late Proterozoic Adamastor Ocean and tectonostratigraphic terrane accretion in southwestern Gondwanaland. International Geological Congress Abstracts 28, 2–35.

Hedberg, R.M., 1979. Stratigraphy of the Ovamboland Basin. South West Africa. Bulletin of the Precambrian Research Unit, University of Cape Town 24, 325.

Hoffman, K.-H., 1994. New constraints on the timing of continental breakup and collision in the Damara Belt. In: Niall, M., McManus, C.

(Eds.), Proterozoic Crustal and Metallogenic Evolution. Abstracts of Geological Society and Geological Survey of Namibia Conference 30, Windhoek.

Hoffman, P.F., Swart, R., Eckhardt, E.F., Guowei, H., 1994. Damara orogen of northwest Namibia. Geological excursion guide of the Geological Survey of Namibia, 55pp.

Hoffman, P.F., Hawkins, D.P., Isachsen, C.E., Bowring, S.A., 1996. Precise U–Pb zircon ages for early Damaran magmatism in the Summas Mountains and Welwitschia Inlier, northern Damara belt, Namibia. Communs Geological Survey Namibia 11, 47–52.

Hoffman, P.F., Kaufman, A.J., Halverson, G.P., Schrag, D.P., 1998. A Neoproterozoic snowball earth. Science 281, 1342–1346.

Holdsworth, R.E., Pinheiro, R.V.L., 2000. The anatomy of shallow-crustal transpressional structures: insights from the Archaean Carajas fault zone, Amazon, Brazil. Journal of Structural Geology 22, 1105–1123.

Holdsworth, R.E., Strachan, R.A., 1991. Interlinked system of ductile strike slip and thrusting formed by Caledonian sinistral transpression in northeastern Greenland. Geology 19, 510–513.

Hudleston, P.J., 1989. The association of folds and veins in shear zones. Journal of Structural Geology 11, 949–957.

Johnson, P.R., Kattan, F., 2001. Oblique sinistral transpression in the Arabian shield: the timing and kinematics of a Neoproterozoic suture zone. Precambrian Research 107, 117–138.

Jones, D.G., Silberling, N.J., Hillhouse, J., 1977. Wrangellia—a displaced terrane in northwestern North America. Canadian Journal of Earth Sciences 14, 2565–2577.

Jones, K.A., Strachan, R.A., 2000. Crustal thickening and ductile extension in the NE Greenland Caledonides: a metamorphic record from anatectic pelites. Journal of Metamorphic Geology 18, 719–735.

Jung, S., Hoernes, S., Mezger, K., 2000. Geochronology and petrology of migmatites from the Proterozoic Damara Belt—importance of episodic fluid-present disequilibrium melting and consequences for granite petrology. Lithos 51, 153–179.

Kamona, A.F., Leveque, J., Friedrich, G., Haack, U., 1999. Lead isotopes of the carbonate-hosted Kabwe, Tsumeb, and Kipushi Pb–Zn–Cu sulphide deposits in relation to Pan African orogenesis in the Damaran–Lufilian fold belt of Central Africa. Mineralium Deposita 34, 273–283.

Kröner, A., 1982. Rb–Sr geochronology and tectonic evolution of the Pan-African belt of Namibia. American Journal of Science 282, 1471–1507.

Lacassin, R., Mattauer, M., 1985. Kilometre-scale sheath fold at Mattmark and implications for transport direction in the Alps. Nature 315, 739–742.

Lin, S., Jiang, D., 2001. Using along-strike variation in strain and kinematics to define the movement direction of curved transpressional shear zones: an example from northwestern Superior Province, Manitoba. Geology 29, 767–770.

Lister, G.S., Snoke, A.W., 1984. S–C mylonites. Journal of Structural Geology 6, 617–638.

Little, T.A., Holcombe, R.J., Ilg, B.R., 2002. Kinematics of oblique collision and ramping inferred from microstructures and strain in middle crustal rocks, central Southern Alps, New Zealand. Journal of Structural Geology 24, 219–239.

Lowell, J.D., 1972. Spitsbergen Tertiary orogenic belt and the Spitsbergen fracture zone. Geological Society of America Bulletin 83, 3091–3102.

Miller, R.Mc.G., 1983. The Pan-African Damara Orogen of Namibia. In: Miller, R.Mc.G. (Ed.), The Damara Orogen, Special Publication of the Geological Society of South Africa 11, pp. 431–515.

Miller, R.Mc.G., Burger, A.J., 1983. U–Pb zircon age of the early Damaran Naauwpoort Formation. Special Publication of the Geological Society of South Africa 11, 267–272.

Miller, R.McG., Grote, W., 1988. Geological map of the Damara Orogen, Namibia, 1:500,000 scale. Geological Survey of Namibia, Windhoek, sheet 1.

Oldow, J.S., Bally, A.W., Ave'L'Lallemant, H.G., 1990. Transpression, orogenic float, and lithospheric balance. Geology 18, 991–994.

Oliver, G.J.H., 1994. Mid-crustal detachment and domes in the central zone of the Damaran Orogen, Namibia. Journal of African Earth Sciences 19, 331–344.

Passchier, C.W., 2001. Flanking structures. Journal of Structural Geology 23, 951–962.

Passchier, C.W., Simpson, C., 1986. Porphyroclast systems as kinematic indicators. Journal of Structural Geology 8, 831–843.

Porada, H., 1979. The Damara–Ribeira Orogen of the Pan-African–Brasiliano cycle in Namibia (Southwest Africa) and Brazil as interpreted in terms of continental collision. Tectonophysics 57, 237–265.

Porada, H., 1989. Pan-African Rifting and Orogenesis in Southern to Equatorial Africa and Eastern Brazil. Precambrian Research 44, 103–136.

Porada, H., Ahrendt, H., Behr, H.J., Weber, K., 1983. The join of the coastal and intracontinental branches of the Damara Orogen, Namibia, South West Africa, Springer-Verlag, Berlin, pp. 901–912.

Prave, A.R., 1996. Tale of three cratons: tectonostratigraphic anatomy of the Damara Orogen in northwestern Namibia and the assembly of Gondwana. Geology 24, 1115–1118.

Ramsay, J.G., 1967. Folding and Fracturing of Rocks, McGraw-Hill, New York.

Ramsay, J.G., 1979. Shear zones. In: Proceedings of Conference 8; Analysis of Actual Fault Zones in Bedrock. U.S. Geological Survey Open-file Report 79-1239, pp. 2–35.

Ramsay, J.G., Graham, R.H., 1970. Strain variation in shear belts. Canadian Journal of Earth Science 7, 786–813.

Ramsay, J.G., Huber, M.I., 1983. The Techniques of Modern Structural Geology. 1. Strain Analysis, Academic Press, London.

Robin, P.-Y.F., Cruden, A.R., 1994. Strain and vorticity patterns in ideally ductile transpression zones. Journal of Structural Geology 16, 447–466.

Seth, B., Kroner, A., Mezger, K., Nemchin, A.A., Pidgeon, R.T., Okrusch, M., 1998. Archaean to Neoproterozoic magmatic events in the Kaoko belt of NW Namibia and their geodynamic significance. Precambrian Research 92, 341–363.

Seth, B., Okrusch, M., Wilde, M., Hoffmann, K.-H., 2000. The Voetspoor Intrusion, Southern Kaoko Zone, Namibia: mineralogical, geochemical and isotopic constraints for the origin of a syenitic magma. Communications of the Geological Survey of Namibia 12, 125–137.

Shackleton, R.M., Ries, A.C., 1984. The relation between regionally consistent stretching lineations and plate motions. Journal of Structural Geology 6, 111–117.

Siendner, G., Mitchell, J.G., 1976. Episodic Mesozoic volcanism in Namibia and Brazil: a K–Ar isochron study bearing on the opening of the south Atlantic. Earth Planetary Science Letters 30, 292–302.

Simpson, C., 1984. Borrego Springs–Santa Rosa mylonite zone: a Late Cretaceous west-directed thrust in southern California. Geology 12, 8–11.

Solar, G.S., Brown, M., 2001. Deformation partitioning during transpression in response to Early Devonian oblique convergence, northern Appalachian orogen, USA. Journal of Structural Geology 23, 1043–1065.

Soper, N.J., Strachan, R.A., Holdsworth, R.E., Gayer, R.A., Greiling, R.O., 1992. Sinistral transpression and the Silurian closure of Iapetus. Journal of the Geological Society, London 149, 871–880.

Swart, R., 1992. The sedimentology of the Zerrissene turbidite system, Damara Orogen, Namibia. Memoir Geological Survey of Namibia 13, 54.

Sylvester, A.G., 1988. Strike-slip faults. Geological Society of America Bulletin 100, 1666–1703.

Sylvester, A.G., Smith, R.R., 1976. Tectonic transpression and basement-controlled deformation in the San Andreas fault zone, Salton Trough, California. American Association of Petroleum Geologists Bulletin 60, 2081–2102.

Tegtmeyer, A., Kroner, A., 1985. U–Pb zircon ages for granitoid gneisses in northern Namibia and their significance for Proterozoic crustal evolution of southwestern Africa. Precambrian Research 28, 311–326.

Teyssier, C., Tikoff, B., 1998. Strike-slip partitioned transpression of the

San Andreas fault system: a lithospheric-scale approach. In: Holdsworth, R.E., Strachan, R.A., Dewey, J.F. (Eds.), Continental Transpressional and Transtensional Tectonics. Geological Society, London, Special Publications 135, pp. 143–158.

Tikoff, B., Greene, D., 1997. Stretching lineations in transpressional shear zones: an example from the Sierrra Nevada Batholith, California. Journal of Structural Geology 19, 29–39.

Tikoff, B., Peterson, K., 1998. Physical experiments of transpressional folding. Journal of Structural Geology 20, 661–672.

Tikoff, B., Teyssier, C., 1994. Strain modeling of displacement-field partitioning in transpressional orogens. Journal of Structural Geology 16, 1575–1588.

Trompette, R., 1997. Neoproterozoic (~600 Ma) aggregation of Western Gondwana: a tentative scenario. Precambrian Research 82, 101–112.

Trompette, R., Carozzi, A.V., 1994. Geology of Western Gondwana (2000–500 Ma). Pan-African–Brasiliano Aggregation of South America and Africa, A.A. Balkema, Rotterdam, Brookfield, 350pp.

Vassallo, J.J., Wilson, C.J.L., 2002. Palaeoproterozoic regional-scale noncoaxial deformation: an example from eastern Eyre Peninsula, South Australia. Journal of Structural Geology 24, 1–24.

Weber, K., Ahrendt, H., 1983. Structural Development of the Ugab Structural Domain of the Northern Zone of the Damara Orogen, Springer-Verlag, Berlin, pp. 699–721.

Wilcox, R.E., Harding, T.P., Seely, D.R., 1973. Basic wrench tectonics. American Association of Petroleum Geologists Bulletin 57, 74–96.

Woodcock, N.H., 1986. The role of the strike-slip fault systems at plate boundaries. Royal Society of London Philosophical Transactions 317A, 13–29.